OULU 2006
C 249

ACTA UNIVERSITATIS OULUENSIS

Matti Kinnunen

COMPARISON OF OPTICAL COHERENCE TOMOGRAPHY, THE PULSED PHOTOACOUSTIC TECHNIQUE, AND THE TIME-OF-FLIGHT TECHNIQUE IN GLUCOSE MEASUREMENTS *IN VITRO*

FACULTY OF TECHNOLOGY,
DEPARTMENT OF ELECTRICAL AND INFORMATION ENGINEERING,
INFOTECH OULU,
UNIVERSITY OF OULU

ACTA UNIVERSITATIS OULUENSIS
C Technica 249

MATTI KINNUNEN

COMPARISON OF OPTICAL COHERENCE TOMOGRAPHY, THE PULSED PHOTOACOUSTIC TECHNIQUE, AND THE TIME-OF-FLIGHT TECHNIQUE IN GLUCOSE MEASUREMENTS *IN VITRO*

Academic Dissertation to be presented with the assent of the Faculty of Technology, University of Oulu, for public discussion in the Auditorium TS101, Linnanmaa, on August 18th, 2006, at 12 noon

OULUN YLIOPISTO, OULU 2006

Acta Univ. Oul. C 249, 2006

Supervised by
Professor Risto Myllylä

Reviewed by
Assistant Professor Torbjörn Löfqvist
Professor Valery V. Tuchin

ISBN 951-42-8145-4 (Paperback)
ISBN 951-42-8146-2 (PDF) http://herkules.oulu.fi/isbn9514281462/
ISSN 0355-3213 (Printed)
ISSN 1796-2226 (Online) http://herkules.oulu.fi/issn03553213/

Cover design
Raimo Ahonen

OULU UNIVERSITY PRESS
OULU 2006

Kinnunen, Matti, Comparison of optical coherence tomography, the pulsed photoacoustic technique, and the time-of-flight technique in glucose measurements *in vitro*

Faculty of Technology, University of Oulu, P.O.Box 4000, FI-90014 University of Oulu, Finland, Department of Electrical and Information Engineering, Infotech Oulu, University of Oulu, P.O.Box 4500, FI-90014 University of Oulu, Finland

Acta Univ. Oul. C 249, 2006
Oulu, Finland

Abstract

The development of a non-invasive glucose monitoring technique is very important because it would tremendously diminish the need to puncture the skin when taking blood samples and help diabetic patients in controlling their blood glucose levels and in treating *Diabetes Mellitus*. The focus of this thesis is on measuring the effect of glucose on the light scattering properties of a tissue-simulating phantom and biological tissues *in vitro*. Optical coherence tomography (OCT), the pulsed photoacoustic (PA) technique, and the time-of-flight (TOF) technique are used in the measurements and their capabilities for detecting changes in the scattering properties are evaluated and compared with each other. The theoretical background of the techniques, light propagation and PA wave generation are briefly explained. The glucose-induced changes in light scattering are also reviewed.

The measurement results with the OCT and the PA technique from Intralipid, pig whole blood, and mouse skin tissue samples show that the glucose-induced changes are larger in the biological tissues than in the Intralipid phantom. The PA measurements show that although the PA signals are stronger at a wavelength of 532 nm than at 1064 nm, the glucose-induced change in the peak-to-peak value of the PA signal measured from pig whole blood is larger at a wavelength of 1064 nm than at 532 nm. The TOF measurements with a streak camera show that the scattering-related changes in the registered pulse shapes occur mainly in the rising part of the pulses. The utilization of fiber-optic measurement heads enabled the detection of back-scattered photons at different distances from the emitting fiber.

Although all the techniques are able to detect changes induced by large glucose concentrations (0–5000 mg/dl) in Intralipid, the effect of glucose on the scattering properties of Intralipid is so weak that the techniques failed to detect changes with lower (50–500 mg/dl) concentrations. The measurements of biological samples with the PA technique and with the OCT also demonstrate capabilities to measure glucose concentrations in the physiologically relevant range (18–450 mg/dl) as well. The results compare well with earlier literature and also confirm some earlier findings.

Keywords: Diabetes Mellitus, glucose measurements, light scattering, optical coherence tomography, photoacoustic measurement, time-of-flight

Acknowledgements

The work in this thesis project continues the studies made with non-invasive glucose monitoring techniques in the Optoelectronics and Measurement Techniques Laboratory at the University of Oulu. I would like to address my warmest thanks to my supervisor Professor Risto Myllylä for focusing the research area and guiding my work during the project. I would also like to thank Zuomin Zhao for his help and guidance.

I would like to thank my co-workers in our laboratory for their helpful assistance and discussions, especially Jukka Hast, Erkki Alarousu, Tuukka Prykäri, Juha Saarela, Tapio Fabritius, Matti Törmänen, and Matti Okkonen.

Special thanks also go to co-workers Professor Alexander Priezzhev, Alexey Popov, Mikhail Kirillin, and Jerzy Pluciński. I also wish to thank Matti Polojärvi, Anssi Rimpiläinen, and Vesa Kaltio for manufacturing special parts for the measurement devices and fiber optic probes. Sergei Vainshtein deserves acknowledgement for helping me in the use of the picosecond laser module and streak camera.

The measurements with blood samples would not be possible without the help of the personnel of the Laboratory Animal Center of the University of Oulu. Thus, I would like to acknowledge them. Special thanks also go to Professor Seppo Vainio, Hannele Härkman, Tiina Jokela, Herkko Sikkilä and the whole personnel of the Department of Medical Biochemistry and Molecular Biology, and the Department of Medical Microbiology in the Faculty of Medicine, University of Oulu. They made the studies with mouse skin samples possible.

Financial support was mainly granted by Infotech Oulu Graduate School and Infotech Oulu. Other financial support was received from the foundations Ulla Tuomisen säätiö, Tekniikan edistämissäätiö, and Oulun yliopiston tukisäätiö. I am very thankful to all of them.

I would like to thank Keith Kosola and Keith Hakso for revising the English of the thesis and Assistant Professor Torbjörn Löfqvist and Professor Valery Tuchin for reviewing the thesis.

Finally, I would like to thank my wife Minna and my children Pihla, Topias, and Joel for their support and patience during this project.

Oulu, May 2006 Matti Kinnunen

List of symbols and abbreviations

c	speed of light in continuum
C_P	specific heat
d	diameter of the acoustic wave
d_s	thickness of the cuvette
D	diffusion coefficient
E	pulse energy of the laser source
E_a	absorbed energy
f	frequency
f_l	focal length of the lens
fs	femtosecond
g	anisotropy parameter
g_{eff}	effective anisotropy parameter
H	function of the heat deposited in the medium per unit volume and time
H_f	laser fluence
I	detected light intensity
$I_d(\tau)$	signal current at the detector
I_r	signal intensity in the reference arm
i_s	total photocurrent
I_s	signal intensity in the sample arm
$i_{T,sb}$	single back-scattered component
$i_{T,ms}$	multiple back-scattered component
I_0	incident light intensity
k	proportional constant
k_l	wave number
l	dimension parameter
$L(\mathbf{r}, \mathbf{s}, t)$	radiance at position **r** travelling in direction **s** at time t
L_p	path length between interactions
m	dimension parameter
m_p	number of particles
n	refractive index
n_p	dimension parameter

nJ	nanojoule
ns	nanosecond
p	the acoustic pressure
P_r	power of the reference beam
P_s	power of the input sample beam
ps	picosecond
$p(\theta)$	scattering phase function
$p(\mathbf{s}', \mathbf{s})$	normalized phase function
r	distance of detection
$\mathbf{r}$	position vector
R	measure of the acoustic source radius
r_i	coordinate
R_r	a pseudorandom number
$\mathbf{s}$	direction vector
$\mathbf{s'}$	direction vector
$S(\mathbf{r},t)$	photon source
t	time
v	velocity of light in the medium
v_a	velocity of acoustic waves
V	volume
$V_{tc}(\tau)$	temporal coherence function
w_0	$1/e$ intensity radius of light beam in the lens plane
z	distance
z_f	border between near field and far field zones
z_i	coordinate
z_0	depth
α	factor for converting power to current
β	volume expansion coefficient
ΔT	temperature change
$\varepsilon(\mathbf{r}, \mathbf{s}, t)$	power radiation of the source per unit volume per unit solid angle in the direction $\mathbf{s}$ at time t
$\phi(\mathbf{r}, t)$	diffuse photon fluence rate
Γ	Grüneisen parameter
λ	median wavelength of the light source in a vacuum
λ_{ac}	acoustic wavelength
μ_a	optical absorption coefficient
μ_{eff}	effective attenuation coefficient
μ_s	optical scattering coefficient
μ_s'	reduced scattering coefficient
μ_t	attenuation coefficient
μJ	microjoule
θ	scattering angle
θ_{rms}	root-mean-square scattering angle
ρ	density
ρ_p	radial position of the detector with respect to the source

$\rho_0(z)$	the lateral coherence length of the reflected sample field in the mixing plane
σ_b	effective back-scattering cross section
τ	time delay
τ_a	stress relaxation time
τ_c	time constant
τ_h	heat diffusion time
τ_L	laser pulse duration
υ_l	frequency of light
Ω	spatial angle

CCD	charge-coupled device
FWHM	full width at half maximum
GI	graded index
IDDM	insulin-dependent diabetes mellitus
IR	infrared
ISF	interstitial fluid
LSP	least scattered photons
MC	Monte Carlo
MCP	microchannel plate
MSP	multiple scattered photons
NAD(P)H	nicotinamide adenine dinucleotide phosphate (reduced)
NIDDM	non-insulin-dependent diabetes mellitus
NIR	near infrared
OA	optoacoustic
OCT	optical coherence tomography
OLCR	optical low-coherence reflectometer
OTDR	optical time-domain reflectometer
PA	photoacoustic
PVDF	polyvinylidenefluoride
PZT	lead zirconium titanate
RBC	red blood cell
RTT	radiative transfer theory
SD	standard deviation
SI	step index
SLD	superluminescence diode
SNR	signal-to-noise ratio
SPA	scattering photoacoustic
TOF	time-of-flight

List of original papers

I Kinnunen M, Popov AP, Pluciński J, Myllylä R & Priezzhev AV (2004) Measurements of glucose content in scattering media with time-of-flight technique; comparison with Monte Carlo simulations. Proceedings of SPIE, Saratov Fall Meeting 2003: Optical Technologies in Biophysics and Medicine V 5474: 181–191.

II Kirillin M, Priezzhev AV, Kinnunen M, Alarousu E, Zhao Z, Hast J & Myllylä R (2004) Glucose sensing in aqueous Intralipid suspension with an optical coherence tomography system: experiment and Monte Carlo simulation. Proceedings of SPIE, Optical Diagnostics and Sensing IV 5325: 164–173.

III Kinnunen M, Zhao Z & Myllylä R (2005) Comparison of the pulsed photoacoustic technique and the optical coherence tomography from the viewpoint of biomedical sensing. Proceedings of SPIE, Optical Materials and Applications 5946: 468–480.

IV Kinnunen M, Zhao Z & Myllylä R (2006) Glucose-induced changes in the optical properties of Intralipid. Optics and Spectroscopy 101 (1): 54–59.

V Kinnunen M & Myllylä R (2005) Effect of glucose on photoacoustic signals at the wavelenghts of 1064 and 532 nm in pig blood and intralipid. Journal of Physics D: Applied Physics 38: 2654–2661.

VI Kinnunen M, Myllylä R, Jokela T & Vainio S (2006) In vitro studies toward non-invasive glucose monitoring with optical coherence tomography. Applied Optics 45 (10): 2251–2260.

VII Kinnunen M & Myllylä R (2006) Comparative study of optical coherence tomography, photoacoustic technique, and time-of-flight technique in phantom measurements. Proceedings of SPIE, Saratov Fall Meeting 2005: Optical Technologies in Biophysics and Medicine VII 6163, in press.

These papers are referred to in the text by Roman numerals I–VII.

Paper I shows time-of-flight (TOF) measurements and simulations with picosecond laser pulses and a streak camera in an Intralipid phantom with different amounts of added glucose. Paper II shows glucose measurements and simulation results in Intralipid with optical coherence tomography (OCT). The author prepared the samples and took part in the measurements and signal analysis in Papers I and II. He also took part in writing

and editing the papers. Paper III is an extensive comparative study of OCT and the photoacoustic (PA) technique in biomedical applications. In Paper III, the part concerning OCT was written by the author, and the combination of different parts and the comparison of the PA technique and OCT were done mainly by the author. Paper IV describes measurements of Intralipid with the PA technique and also with optical methods with different glucose concentrations. Paper V shows glucose measurements with the PA technique in Intralipid and pig whole blood. In Paper VI, OCT measurements were taken in Intralipid and in cultured mouse skin samples with different glucose concentrations. In Papers IV, V, and VI the samples were prepared and the experiments were taken by the author. Finally, Paper VII contains a comparison of the three techniques (OCT, PA and TOF). The comparison of the techniques in Paper VII as well as the writing of Papers IV-VII were mainly done by the author. The finalization of the publications was made together with all the authors. This thesis is based on the above publications. Moreover, some unpublished data is included in the thesis.

Contents

1 Introduction

1.1 Overview and motivation

Diabetes Mellitus is a disorder of glucose metabolism in which the secretion of insulin is prevented (insulin-dependent diabetes mellitus (IDDM), type 1) [1], or the cells of human tissue are unable to use insulin (non-insulin-dependent diabetes mellitus (NIDDM), type 2). These problems induce great difficulties in controlling the blood glucose level. Millions of people around the world suffer from *Diabetes Mellitus* [2,3]. To ensure proper treatment of the disorder, the blood glucose concentration has to be measured several times a day. At the moment, people suffering from diabetes need to puncture their skin to take a blood sample for measuring their blood glucose level. The current techniques use test strips and are based on glucose oxidation or an electrochemical method [4,5]. Also minimally invasive techniques, such as microneedles that utilize sweat and saliva have been developed [6]. In addition, implantable sensors as well as sensors based on reverse iontophoresis are under investigation [7,8]. Continuous glucose monitoring helps people suffering from diabetes monitor rapid fluctuations in their blood glucose level and facilitates proper treatment of the disease [9,10]. Proper control of the blood glucose level is the key to minimizing further complications of *Diabetes Mellitus* [11]. Also, infants and older people in hospitals need regular control of their blood glucose level. Thus, there is a great demand for a non-invasive blood glucose monitoring technique.

Non-invasive measurement techniques for measuring the glucose concentration of the human body have been developed over the past twenty years. During the past decade, the focus has largely been on optical techniques based on the interactions of photons with the object being studied. One of the biggest advantages of optical techniques, when using moderate optical power, is that they are harmless to the objects being studied.

The photoacoustic technique (PA), optical coherence tomography (OCT) and near infrared spectroscopy (NIR) are examples of the latest and most studied techniques for non-invasive glucose monitoring. These techniques have been applied both *in vitro* and *in vivo*. OCT has shown promising results over the past few years for continuous glucose monitoring. However, all these techniques need calibration with invasively taken blood samples.

1.2 Objectives

In this thesis, three different techniques and their possibilities for non-invasive glucose monitoring *in vitro* are compared. The aim is to get information about the effect of changing scattering properties on the measured signal parameters with OCT, PA and time-of-flight (TOF) techniques at different wavelengths. These parameters are OCT signal slope value, PA signal peak-to-peak value, and TOF signal pulse amplitude, pulse width, and time of arrival of the pulse maximum. Moreover, the glucose-induced changes in the light scattering properties are measured with these techniques in Intralipid phantoms, in pig whole blood, and in cultured mouse skin samples. The content of this thesis will add additional information to the literature of non-invasive glucose monitoring with OCT, PA and TOF techniques *in vitro*, and will also confirm a few earlier observations achieved with different techniques.

1.3 Outline of the dissertation

The basic principles of optical and PA techniques used in non-invasive glucose monitoring are introduced in Chapter 2. These techniques are NIR spectroscopy, infrared (IR) spectroscopy, spatially resolved diffuse reflectance measurements, polarimetry, Raman spectroscopy, fluorescence, PA and optoacoustic (OA) techniques, and OCT. This chapter also contains some notes on non-invasive glucose monitoring, and a review of the literature concerning glucose studies with OCT, PA, and TOF techniques *in vitro*.

The theoretical background of light scattering studies with TOF, PA, and OCT techniques is described in Chapter 3. These include the radiative transfer theory (RTT) in section 3.1, PA wave generation in section 3.2, and the formation of the OCT signal in section 3.3. This chapter also describes the basics of Monte Carlo (MC) simulation. Moreover, the literature concerning glucose-induced changes in scattering is reviewed in section 3.4.

Chapter 4 contains a brief description of the basics of the measurement techniques used in this study (OCT, PA and TOF). The use of optical fibers is introduced in section 4.3.1 and the techniques are compared in section 4.4.

The basic results of the *in vitro* studies carried out during this thesis work are summarized in Chapter 5. Section 5.4 includes a discussion on the results and an introduction to some future work.

Finally, the results are summarized and a conclusion is drawn in Chapter 6.

2 Non-invasive glucose monitoring

2.1 Glucose in the human body

D-glucose is a molecule with the chemical formula $C_6H_{12}O_6$. It is the basic energy source for cellular metabolism. Glucose concentration varies between different anatomic regions and in different parts of the blood circulation. The daily variation of glucose concentration in the human body is in the range of 18–450 mg/dl, being typically in the range of 70–160 mg/dl [12]. Glucose permeates red blood cells (RBCs) via passive-mediated diffusion, which is supported by 55-kD-glycoprotein [13]. RBCs work as a buffer in blood to control the plasma glucose concentration [14].

It is suspected that D-glucose does not need a transporter to move between blood plasma and interstitial fluid (ISF). This process is thought to be driven by diffusion gradients. When the glucose concentration of plasma increases, the initial response is water movement from ISF to plasma; then the glucose diffuses into the ISF, where it is used as an energy source by cells. Because of these gradients, the glucose concentration in tissues is not a constant. The glucose concentration is higher in arterial blood than in venous blood, and the venous glucose concentration depends on the arterial blood flow rate and the rate of glucose uptake by the tissue. [14]

Unlike between blood plasma and ISF, there are many glucose transporters through the cell membrane. The transport process of glucose is called passive-mediated or facilitated diffusion. In many organelles these transporters are stimulated by insulin. The distribution of the transporters varies between organelles. The transport rate of glucose into cells is possibly limited by glucose transporters or by glucose phosphorylation. [13,14]

It is not known whether there is free glucose inside the cells or only phosphorylated products of glucose. In muscle cells, the glucose is phosphorylated rapidly after the intake into the cell. [14]

Although many body fluids and tissues have been studied for non-invasive glucose sensing, in the best case scenario, the blood glucose concentration would be measured directly from the blood vessels. To make a diagnosis of *Diabetes Mellitus*, the vein plasma glucose should be measured [15].

2.2 Basics of optical and photoacoustic measurement techniques

Optical techniques are based on analysing photon propagation and distribution inside the sample. Different properties of light are measured and the effect of glucose on the collected signals is evaluated with different techniques. Bruulsema *et al*. [16] and Heinemann *et al*. [17] have studied the effect of glucose on optical properties. Glucose affects light scattering and also, to some extent, light absorption. The most pronounced effect of increased glucose concentration is decreased scattering. Non-invasive measurement techniques have been reviewed by several researchers: Heise [18], Coté [19], Waynant *et al.* [20], Khalil [21,22], and McNichols *et al*. [23]. The most common techniques are NIR and IR spectroscopy, spatially resolved diffuse reflectance measurements, polarimetry, Raman spectroscopy, PA and OA techniques, and OCT.

2.2.1 Near infrared spectroscopy

NIR spectroscopy is based on collecting reflectance or absorption spectra of the tissue with a spectrometer. Continuous light is used to illuminate the tissue under study. A typical wavelength range is 1050–2450 nm. [24] The spectrometric techniques enable the study of glucose absorption bands in this wavelength range. NIR spectroscopy has been studied extensively in the last decade. Marbach *et al.* [25] used NIR spectroscopy to measure blood glucose from the human inner lip and Malin *et al*. [24] for measuring blood glucose. The NIR technique has also been critically examined by Arnold [26]. Moreover, this technique is under continuous development [27,28].

2.2.2 Infrared spectroscopy

IR spectroscopy uses wavelengths between 2.5–20 μm. It is based on studies of light absorption by glucose at a selected wavelength range. The absorption spectrums are collected with a spectrophotometer. [29] Zeller *et al.* [29], Mendelson *et al.* [30] and Klonoff *et al.* [31] have measured blood glucose concentration with IR spectroscopy.

2.2.3 Spatially resolved diffuse reflectance measurements

Glucose monitoring with a spatially resolved diffuse reflectance measurement technique is based on detecting changes in the tissue's reduced scattering coefficient (μ_s'). In this technique, the incoming light beam is directed into the tissue and diffusely reflected light is collected at different distances from the location of the incoming radiation. The μ_s' can be deduced by using a diffuse model to fit the measured signal profiles with the theoretical model. Bruulsema *et al.* [16,32] have studied the feasibility of this technique for non-invasive glucose monitoring, and this technique has been studied further by Heinemann *et al*. [17,33].

The recent results by Khalil *et al*. [34] measured with the spatially resolved diffuse reflectance technique show that temperature affects the cutaneous μ_s' and absorption coefficient (μ_a) values. Cutaneous μ_s' shows linear changes as a function of temperature whereas the changes in μ_a showed complex and irreversible behaviour. The thermal response of skin has been used as a basis for non-invasive differentiation of normal and diabetic skin [35].

2.2.4 Polarimetry

Polarimetry is an optical technique based on detecting the rotation angle of linearly polarized light. Glucose molecules can rotate the polarization plane. The rotation angle is linearly proportional to the optical path length, glucose concentration and a specific rotation coefficient. [36] Chou *et al*. [37] used polarimetry to detect aqueous glucose in a rabbit's eye. It has typically been used to measure the glucose content of aqueous humor in the eye by using a tangential optical path. Also, a different measurement scheme using Brewster reflection has been reported [38].

2.2.5 Raman spectroscopy

The basics of Raman spectroscopy can be explained as follows: part of the photons travelling in the sample scatter with a shift in photon energy. This shift occurs during inelastic collision, when photon energy transfers to or from the molecule. By analysing the resulting spectra of Raman scattering it is possible to get information about the chemical structure (including glucose) of the medium. [39] Berger *et al*. [40,41] and Goetz *et al*. [42] have used Raman spectroscopy to detect glucose. Data recently published by Enejder *et al*. [43] demonstrate the feasibility of Raman spectroscopy in monitoring blood glucose *in vivo*.

2.2.6 Fluorescence

There have been developments in the fluorescence-based glucose sensors over the past few years. The results in papers by Pickup *et al*. [10,44] show that intrinsic tissue fluorescence could possibly be used as a basis for non-invasive glucose monitoring. This technique is based on the detection of the fluorescent cofactor nicotinamide adenine dinucleotide phosphate (reduced) (NAD(P)H), a product of glucose metabolism. NAD(P)H has fluorescence at a wavelength of 440–480 nm, when exciting at 340 nm. Fluorescence-based sensors are very sensitive and they can even measure glucose at the molecular level. They have been tested in *in vitro* models and they need to be studied in *in vivo* conditions. Both fluorescence intensity and lifetime detection need further investigation. [44]

2.2.7 Photoacoustic and optoacoustic techniques

The PA technique is based on the detection of pressure waves generated by absorbing photons. A conventional method for studying gases and liquids is to generate pressure waves with a continuous wave light source and a chopper [45]. Another possibility is to use pulsed light, such as pulsed lasers, as an energy source. This is the case in the rest of this thesis.

Nanosecond (ns) range optical pulses are used to induce a rise in temperature, and thus a volumetric expansion inside the studied sample. The pressure waves generated this way can be detected with acoustic or optical detectors. The optical detectors are based, for example, on a probe-beam deflection method or on an interferometer [46]. In the probe-beam deflection method the probing light beam deflects when travelling through a region of refractive index change affected by the PA pulses. The interferometer, on the other hand, is very sensitive in detecting PA pulse-induced pressure changes on the surface of the sample. The detection of glucose with the PA technique is based on registering the changes in the peak-to-peak value of the signal, whereas the OA technique is based on analysing changes in the exponential curve fitted to the time-domain pulse profile. The PA and OA techniques have been used to measure the glucose content of the human body and blood vessels [47-52]. However, some additional technique or information is still needed to make the glucose measurements more precise [49].

2.2.8 Optical coherence tomography

OCT is based on the detection of back-scattered photons with an interferometer. The interferometer consists of sample and reference arms, a light source and a detector. The scanning mechanism in the reference arm enables the detection of photons from different depths in the sample. The glucose sensing is based on analysing changes in the slope value fitted to the OCT signal depth profile. Esenaliev *et al.* [53] and Larin *et al.* [54-56] have used OCT for non-invasive glucose monitoring both *in vitro* and *in vivo*.

2.3 Problems in scattering-based techniques

Increasing glucose concentration decreases the refractive index mismatch between the scattering particles and the base medium, and thus changes the scattering properties. The scattering-based measurement techniques do not measure the glucose directly, but indirectly via its effect on the refractive index [33]. The increase of water concentration in tissue also reduces the scattering by diluting the scattering particle concentration, which may result in a similar change in the measured signal.

When monitoring glucose, the changes in the registered signals have to be examined with great care because the daily variation of human body metabolism also affects the signals in *in vivo* measurements. Larin *et al*. [12] have shown that, although many body

osmolytes change the refractive index mismatch, the effect of glucose on the total refractive index is from 1 to 2 times greater.

Temperature also affects the optical scattering measurements, which makes the glucose measurements more difficult. *In vitro* measurements show that a 1 °C change in temperature equals a 0.2 mM change in glucose concentration [57]. *In vivo* measurements by Khalil *et al.* [34] show that a 1 °C change in the temperature of the cutaneous tissue may increase the μ_s' by a value equalling a glucose change from 5.8 to 11.6 mmol/l.

Moreover, during long measurement periods, such as an oral glucose tolerance test, the probe-skin contact may induce drifts in the μ_s' and μ_a values [34], and thereby make the glucose measurements difficult.

2.4 Glucose measurements *in vitro* with OCT, PA, and TOF techniques

Non-invasive glucose monitoring techniques have been studied a lot *in vitro* in different kinds of phantoms. Next, the focus is on the OCT, PA and TOF techniques.

The effect of glucose on scattering properties has been studied in polystyrene microspheres with OCT at a wavelength of 830 nm [56] and in polystyrene microspheres and milk phantoms at a wavelength of 1300 nm [56,58,59]. With the PA technique, the glucose-induced changes have been studied for example in an aqueous water solution at wavelengths of 800–1200 nm [49], 1700 nm [50], and 9676 nm [47], in gelatin-based tissue phantom with an immersed capillary tube with water-glucose solution at wavelengths of 0.75–1.75 μm [48], and in milk phantoms at a wavelength of 905 nm [60].

Moreover, *in vitro* studies have been conducted in different kinds of biological samples. OCT has been used to measure the refractive index matching effect in blood, especially by using an immersion method [61,62]. The PA technique has been used to measure the effect of glucose on pork meat at a wavelength of 905 nm [60], on human whole blood at wavelengths of 905 nm [63] and 9676 nm [47], and on human plasma at wavelengths of 1180 and 1700 nm [64], whereas the OA technique has been used to measure the effect of glucose on aqueous water-glucose suspensions at wavelengths of 1450 nm and 2150 nm [65], and sheep blood at wavelengths of 532 nm and 1064 nm [52]. TOF measurements have been taken to measure the effect of glucose on blood *in vitro* at a wavelength of 906 nm [66].

A study of the effect of glucose-induced changes on the optical properties of Intralipid has been carried out earlier with a continuous wave light and reflectance measurements [57], but no literature was found concerning Intralipid phantom measurements with different glucose concentrations with OCT, PA and TOF techniques. Because of the easy preparation of the Intralipid samples with different concentrations, as well as the finding that an increasing Intralipid concentration mainly affects the scattering properties [67], it serves as an appropriate medium for investigating and comparing scattering-dependent changes in the signals of different techniques.

Although a study with the OA technique at wavelengths of 532 nm and 1064 nm was done, it was focused on the dynamic properties of glucose-induced changes in blood with

high glucose concentrations. No literature was found concerning measurements of glucose-induced changes in the peak-to-peak values of the PA signal from blood at these wavelengths.

The literature concerning the OCT-based glucose monitoring technique shows that this technique has been applied to homogeneous sample materials *in vitro* as well as to animal and human studies *in vivo*. No earlier glucose studies with the OCT with biological samples *in vitro* were found.

3 Theoretical basics

Chapter 3 gives a short introduction to the theoretical background of light propagation in tissues and tissue-simulating phantoms. Some essential aspects for understanding the basics of the measurement techniques are highlighted. In section 3.1 the basic optical coefficients and the radiation transfer theory (RTT) are described. Section 3.2 explains the basics of PA wave generation, whereas section 3.3 describes the formation of the OCT signal. Next, the glucose-induced changes in scattering are described in section 3.4 and finally, the properties of the used materials are summarized in section 3.5.

3.1 Light propagation in tissues and tissue-simulating phantoms

3.1.1 Parameters describing the interaction of light with matter

The interaction of light with matter is typically described with four parameters: absorption coefficient (μ_a), scattering coefficient (μ_s), anisotropy parameter (g), and refractive index (n). These parameters are macroscopic parameters and they provide an averaged description of the processes occurring in the media. These parameters are wavelength dependent. This allows the utilization of spectroscopic techniques to get information about the different components in a material.

μ_a gives the probability of an absorption event occurring. The unit 1/cm describes how many absorption events occur in the path length of 1 cm. An absorption process requires an appropriate energy level in the sample, which can take the energy of a photon.

μ_s gives the probability of a scattering event occurring. The unit 1/cm describes how many scattering events occur in the path length of 1 cm.

g has been used to specify the direction of the scattering photons. When $g = 1$, it indicates fully forward scattering events, whereas $g = -1$ indicates backward scattering. The g can be defined as the mean cosine of the scattering angle θ [68]:

$$g = \langle \cos\theta \rangle = \int_0^{\pi} p(\theta) \cos\theta \cdot 2\pi \sin\theta d\theta \,. \tag{1}$$

The θ is dependent on the scattering phase function *p(θ)*.

The *n* is defined as the ratio of light velocity in a vacuum (*c*) and in a medium (*v*) [69]:

$$n = c / v \,. \tag{2}$$

3.1.2 Radiative transfer theory

The RTT has been developed to describe energy transfer and light scattering processes in a highly scattering medium. This theory does not include diffraction effects. It is assumed that there are non-correlating fields in the RTT, and hence, the addition of powers holds. [70] This theory is applicable both for continuous and pulsed light. The radiative transfer equation describes light propagation in a scattering sample. The exact solution of this equation can be achieved only in a few cases [70]; therefore different methods and models have been developed to solve this equation and extract the optical coefficients from measured signals. These methods include the Kubelka-Munk theory, the diffusion theory, the adding-doubling method, and the MC simulation method. [71,72] Equation (3) shows a non-stationary version of the radiative transfer equation [70], [I]:

$$\begin{aligned} \frac{1}{v}\frac{\partial L(\mathbf{r},\mathbf{s},t)}{\partial t} &= -\vec{s}\cdot\nabla L(\mathbf{r},\mathbf{s},t) - \mu_a L(\mathbf{r},\mathbf{s},t) - \mu_s L(\mathbf{r},\mathbf{s},t) \\ &\quad + \mu_s \int_{4\pi} p(\mathbf{s}',\mathbf{s}) L(\mathbf{r},\mathbf{s}',t) d\Omega + \varepsilon(\mathbf{r},\mathbf{s},t), \end{aligned} \tag{3}$$

where $L(\mathbf{r}, \mathbf{s}, t)$ is the radiance at position **r** travelling in direction **s** at time *t*; $p(\mathbf{s}', \mathbf{s})$ is the normalized phase function representing the probability of scattering into direction **s'** from direction **s**; Ω is the spatial angle, and $\varepsilon(\mathbf{r}, \mathbf{s}, t)$ is the power radiation of the source per unit volume per unit solid angle in the direction **s** at time *t*.

In many cases analytical solutions to the RTT can be obtained by the diffusion approximation [73]:

$$\frac{1}{v}\frac{\partial}{\partial t}\phi(\mathbf{r},t) - D\nabla^2\phi(\mathbf{r},t) + \mu_a\phi(\mathbf{r},t) = S(\mathbf{r},t) \,, \tag{4}$$

where $\phi(\mathbf{r},t)$ is the diffuse photon fluence rate, *D* is the diffusion coefficient;

$$D = \left\{3\left[\mu_a + (1-g)\,\mu_s\right]\right\}^{-1}, \tag{5}$$

and $S(\mathbf{r},t)$ is the photon source. This approximation is valid, if $\mu_a << (1\text{-}g)\mu_s$, the sample is semi-infinite and homogeneous, and the distance from the light source and detector as well as from the boundaries is sufficiently long [73,74].

Diffusion approximation can also be used to describe the interaction of light pulses with a highly scattering material. The reflected intensity can be calculated from the equation (6) [73]:

$$R(\rho_p,t) = (4\pi Dc)^{-3/2} z_0 t^{-5/2} \exp(-\mu_a ct) \exp(-(\rho_p^2 + z_0^2)/4Dct)\,, \tag{6}$$

where ρ_p is the radial position of the detector with respect to the source and z_0 is the depth ($z_0 = [(1\text{-}g)\,\mu_s]^{-1}$). The time-resolved diffuse reflectance profiles enable the calculation of μ_a and μ_s of the sample from the measured pulse profiles [73,74].

On the other hand, the transmitted light pulses through the sample in a slab cuvette can be described with the equation (7), where d_s is the thickness of the cuvette [73]:

$$\begin{aligned} T(\rho_p,d_s,t) = {} & (4\pi Dc)^{-3/2} t^{-5/2} \exp(-\mu_a ct) \exp\left(-\frac{\rho_p^2}{4Dct}\right) \\ & \times\left\{(d_s - z_0)\exp\left[-\frac{(d_s - z_0)^2}{4Dct}\right] - (d_s + z_0)\exp\left[-\frac{(d_s + z_0)^2}{4Dct}\right]\right. \\ & \left. +(3d_s - z_0)\exp\left[-\frac{(3d_s - z_0)^2}{4Dct}\right] - (3d_s + z_0)\exp\left[-\frac{(3d_s + z_0)^2}{4Dct}\right]\right\}. \end{aligned} \tag{7}$$

3.1.2.1 Monte Carlo simulation

The MC simulation model has been developed to describe light propagation in a tissue. In every interaction point of photons in the medium, the photons are assumed to deposit a fraction of their current weight (initial value was 1) as an absorbing energy. The direction of the scattering photon is selected randomly and the path length between interactions (L_p) is calculated with the formula: $L_p = -\ln(R_r)/\mu_t$, where $0 < R_r < 1$ is a pseudorandom number with an uniform distribution and the attenuation coefficient $\mu_t = \mu_a + \mu_s$. [75]

The solving of RTT with the MC simulation is based on computing random pathways of a large number of photons injected into the sample. The MC simulation needs the optical parameters of the medium (μ_a, μ_s, g, and n) as input values. The number of photons launched affects the signal-to-noise ratio (SNR) of the results as well as the simulation time.

3.1.3 Distribution of photons in the sample

3.1.3.1 Spatial distribution

The shape of the spatial photon distribution depends on the optical properties of the sample, especially μ_s and g. In homogeneous and non-scattering material, the energy density is highest in the center of the light beam, whereas the scattering broadens the photon distribution and decreases the light intensity in the center of the beam.

The light spatial intensity distribution is at a maximum beneath the sample surface in a turbid medium with conditions of $\mu_a << \mu_s$. This maximum originates from the diffuse reflection of the radiation scattered from deeper layers in the medium and also recycling of photons in the sample, and is located at a depth of $\sim 1/\mu_s'$. [76-78]

Information on the spatial distribution of photons is needed in photodynamic therapy to guide the optical energy directly into tumors [79]. This information is typically based on the estimated optical coefficients and simulated light distributions. For a more accurate and direct estimation of optical coefficients, digital video cameras have been used to take light distribution images and to compare with MC simulations [80].

3.1.3.2 Temporal distribution

When a light pulse is entered into the sample, some of the photons are able to travel straight through the sample. These photons form the ballistic or coherent component of the transmitted pulse [81,82]. Some of the photons scatter a few times and form a snake or partially coherent component of the photons' TOF distribution. Most of the photons scatter many times and they form a diffuse component of the photons' TOF distribution. Temporal laser pulse shapes have been used to develop imaging techniques. [81] Some of the photons are absorbed into the sample and cannot be detected at all. Fig. 1 [VII] shows the different components of a transmitted laser pulse. Changes in the optical properties of the material affect the photons' flight time and the lengths of the photon trajectories, changing the shape of the photons' TOF distribution. The back-scattered photons, detected in reflectance measurements, have their own temporal distribution in which the ballistic component is absent.

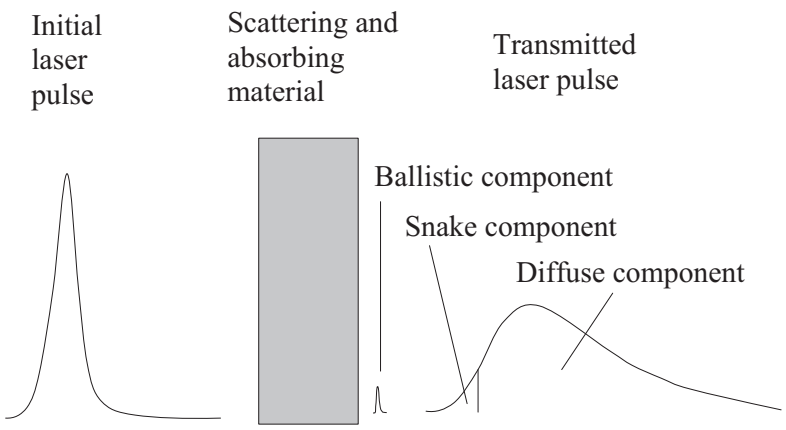

Fig. 1. Effect of scattering and absorption on the transmitted laser pulse shape [VII].

3.2 Photons as an acoustic source

3.2.1 Photoacoustic effect

The formation of PA waves can be described by the wave equation (8) [83], when heat conduction time is long compared with the transit time of sound across the acoustic source, and when viscous effects can be neglected.

$$\left(\nabla^2 - 1/v_a^2 \ *\left(\partial^2/\partial t^2\right)\right) p = -\left(\beta/C_p\right)*\left(\partial H/\partial t\right), \tag{8}$$

where H is a function of the heat deposited in the medium per unit volume and time, p is the acoustic pressure, β is the volume expansion coefficient, C_p is the specific heat at constant pressure, and v_a is the velocity of acoustic waves in the medium. This equation does not consider the scattering effects. The exact theory of the PA effect is described in Refs. [46] and [83].

The most common mechanism for producing PA waves in biomedical applications is the thermal-elastic mechanism. In this mechanism, the energy of photons is converted into heat by a non-irradiative relaxation. The temperature increase causes a volumetric expansion in the heated region, and further, pressure waves. Next is an explanation of the basic concepts of PA wave generation via a semi-quantitative description.

The temperature rises according to:

$$\Delta T = \frac{E_a}{C_P \rho V}, \tag{9}$$

where ρ is density in the optically absorbed volume V, and E_a is the absorbed energy. The temperature rise induces changes in the pressure as follows:

$$\begin{aligned}\Delta P &= \rho v^2 \cdot \beta \Delta T \\ &= \left(\frac{\beta v_a^2}{C_P}\right) \cdot \left(\frac{E_a}{V}\right) = \Gamma H_f \mu_a .\end{aligned} \tag{10}$$

The expression $\beta v_a^2/C_P$ is a temperature function that depends on the produced thermal energy that is being converted into mechanical stress, known as the Grüneisen parameter Γ. E_a/V is the absorbed optical energy density and equals the product of the laser fluence H_f and μ_a.

The PA amplitude can be described by [84]:

$$P = k\left(E \mu_a \beta v_a^{n_p}\right) / \left(C_p r^m R^l\right), \tag{11}$$

where E is the pulse energy of the laser source, R is a measure of the acoustic source radius, r is the distance of detection and k is a proportional constant. l is in the region 0–2 and m is in the region 0–1 relating to the shape of the acoustic source. n_p is in the region of 0.5–2 relating to the duration of the laser pulse.

The conditions for stress confinement have to be met in PA wave generation. In scattering-dominated media, these include the following requirements: a) stress has to be limited to the thermal elastic expansion volume and must not be allowed to relax during irradiation, b) $\tau_a >> \tau_L$ and $\tau_a >> \tau_h$ (τ_a is the stress relaxation time (the time it takes for sound to propagate through the thickness ($1/\mu_{eff}$) of the irradiated region), τ_L is the laser pulse duration and τ_h is the heat diffusion time) or $\mu_{eff} v_a \tau_L << 1$. [51,85] μ_{eff} is the effective attenuation coefficient ($\mu_{eff} = \sqrt{3\mu_a(\mu_a + \mu_s')}$). Fig. 2 shows an example of a PA signal.

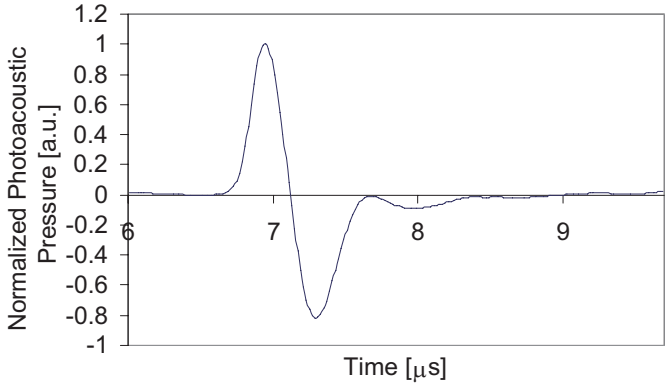

Fig. 2. Normalized photoacoustic signal.

Zhao *et al.* [86] have studied the scattering effects on laser pulse shape and acoustic wave generation. They found that optical scattering decreases the pulsed acoustic intensity in a weakly absorbing media. Optical scattering has a smaller effect on the pulsed acoustic signal than on the optical signal. Scattering broadens the PA source, decreases the energy density, and increases the duration of the PA signal in strongly scattering and weakly absorbing media.

3.2.2 Shape of the acoustic source

The shape of the acoustic source depends on the optical absorption and scattering properties of the sample. In strongly absorbing materials, such as blood, the photons are absorbed quickly. If the penetration depth is much shorter than the diameter of the laser pulse radiation, the acoustic source is plane wave-like. If the laser beam penetration depth equals the laser beam diameter, the shape of the acoustic source is spherical. In a weakly absorbing suspension, the light penetration depth is much greater than the beam diameter of laser pulse radiation, and hence the shape of the sound source is more cylindrical. [84] If the laser pulse duration is much shorter than the transit time of an acoustic wave, the pressure profile of the PA or OA signal mimics the spatial distribution of the heat sources in the medium [76,77].

3.2.3 Propagation of acoustic waves

Acoustic waves attenuate when they propagate in a scattering and absorbing material. Many times absorption and scattering coefficients are combined into an attenuation coefficient [85]. The viscosity and thermal conductivity affect the sound attenuation in a liquid. [51,87] The absorption coefficient of acoustic waves in liquids is proportional to the frequency by $\sim f^2$ [84,85,87], being slightly higher at frequencies smaller than 3 MHz. The acoustic attenuation is quite moderate in the frequency range from 10 kHz to 1 MHz [84,85], and does not limit the usability of the PA technique.

In the pulsed PA technique, the laser pulses generate a wide spectrum of ultrasonic waves. The acoustic pulses expand during propagation due to the larger absorption of the high-frequency components [87]. Diffraction, too, affects the acoustic pulses, and may distort the temporal pulse shape [88]. The diffraction effects are the most pronounced for the low frequency acoustic waves [85].

In the near acoustic field ($z < z_f$, where $z_f = d^2/4\lambda_{ac}$ and $d/2 > \lambda_{ac}$ (z_f is the border between near field and far field zones, λ_{ac} is the acoustic wavelength and d is the diameter of the acoustic wave)) the pressure waves are assumed to be plane waves, whereas in the far acoustic field ($z > z_f$) the pressure waves can be modelled as spherical waves [87].

3.3 Formation of the OCT signal

In OCT, the interference signal is formed at the detector by photons arriving from the sample arm and from the reference arm if the path length difference of the photons is shorter than the coherence length of the light source. The signal current at the detector can be derived to the form [89]:

$$I_d(\tau) = I_s + I_r + 2(I_s I_r)^{1/2} \left|V_{tc}(\tau)\right| \cos(2\pi \upsilon_l \tau), \tag{12}$$

where I_s and I_r are the signal intensities in the sample and reference arms, respectively, $V_{tc}(\tau)$ is the temporal coherence function, υ_l is the frequency of light, and τ is the time delay. By changing the length of the reference arm, it is possible to get information from different depths from the sample.

3.3.1 Single and multiple scattering

The OCT signal consists of single and multiple scattered photons [90]:

$$\left|i_s(r,z)\right| = \left|i_{T,sb}\right| + \left\langle i_{T,ms}^2 \right\rangle^{1/2} = \left|\sum_{i=1}^{m_p} i_{sb}(r_i, z_i)\right| + \left\langle \sum_{i=1}^{m_p} i_{ms}^2(r_i, z_i) \right\rangle^{1/2}, \tag{13}$$

where i_s is the total photocurrent, $i_{T,sb}$ is the single back-scattered component, $i_{T,ms}$ is the multiple back-scattered component, and m_p is the number of particles. (r_i,z_i) denotes the coordinates of the ith particle. The single or least scattered and multiple scattered components can be referred to as LSP and MSP, respectively [91]. The LSP signal contains both single back-scattered photons and MSPs with very small angle forward scattering [91]. The LSPs mainly form the real information of the OCT signal whereas MSPs degrade contrast and resolution [91].

The modelling of the OCT signal has been developed by several researchers [89,90,92-95]. A simple model, which takes into account only the single or least scattered photons, is based on the attenuation of ballistic photons and can be described with the Lambert-Beer law [72]:

$$I = I_0 e^{-\mu_t z}, \tag{14}$$

where I_0 is the incident light intensity, and I is the detected light intensity. In a strong scattering case, when $\mu_a << (1\text{-}g)\mu_s$, μ_t can be replaced with μ_s.

The latest advancements, using the extended Huygens-Fresnel principle [92-94], take into account both the LSP and MSP parts. In this model, the mean square heterodyne signal current can be expressed in the form [92]:

$$\left\langle i^2(z)\right\rangle = \frac{\alpha^2 P_R P_S \sigma_b}{\pi w_H^2} \times \left\{ \exp(-2\mu_s z) + \right.$$

$$\left. \frac{2\exp(-\mu_s z)\left[1-\exp(-\mu_s z)\right]}{1+w_S^2/w_H^2} + \left[1-\exp(-\mu_s z)\right]^2 \frac{w_H^2}{w_S^2} \right\}. \quad (15)$$

The first term ($\alpha^2 P_R P_S \sigma_b / \pi w_H^2$) is the mean heterodyne signal current in a non-scattering medium, where α is a factor for converting power to current, P_R is the power of the reference beam, P_S is the power of the input sample beam, and σ_b is the effective back-scattering cross section. The first term in the brackets is a single scattering term, the second term is a cross term, and the third term is a multiple scattering term. The following equations hold true in cases where the focal plane coincides with the tissue discontinuity [92]:

$$w_H^2 = \left(\frac{f_l}{k_l w_0}\right)^2, \quad (16)$$

$$\frac{w_H^2}{w_S^2} = \frac{1}{1+\left[\frac{2w_0}{\rho_0(z)}\right]^2}, \quad (17)$$

where f_l is the focal length of the lens in the sample arm, $k_l=2\pi/\lambda$ (where λ is the median wavelength of the light source in a vacuum), w_0 is the $1/e$ intensity radius of the light beam in the lens plane, and $\rho_0(z)$ is the lateral coherence length of the reflected sample field in the mixing plane.

The OCT signal attenuation has been studied by several researchers [90,96] both with experiments and with MC simulation. The measurement and MC simulation results show that in the medium with higher scattering the OCT signal attenuates quicker than with lower scattering. The multiple scattering also affects the collected signal at lower depths in a higher scattering medium. [91]

3.4 Glucose-induced changes in scattering

Glucose increases the *n* of the bulk material [97]. At the same time, the refractive index mismatch between scattering particles and the bulk material decreases, and hence the scattering properties of the material decrease. This well-known effect has been studied in different kinds of tissue-simulating phantoms, such as Liposyn-glucose solution and polystyrene microspheres with different diameters [98-100]. Typically a continuous wave

light source and a spectrometer have been used in the measurements. The effect of glucose both on the light absorption and scattering depends on the wavelength [99].

Intralipid has also been used as a sample medium. Glucose decreases the values of the μ_s' and the μ_a of Intralipid, the change being larger in scattering than in absorption [57]. In addition, the scattering is influenced by the size of the scattering particles relative to the wavelength. Increasing the n also decreases the light velocity in the sample. In the NIR spectral region, scattering dominates absorption, which is an advantage in scattering-based glucose monitoring [98].

The photon path lengths become shorter when the glucose concentration increases and scattering decreases [101]. At the same time, the shape of the photons' spatial distribution and the acoustic sound source becomes more cylindrical and the radius of the laser beam in the sample decreases [86]. This change in the energy density of the sample can be seen as an increased peak-to-peak value of the PA signal.

Glucose-induced changes in light transport were studied by Qu *et al*. [102] with MC simulations. They studied the effect of glucose on diffuse transmittance and reflectance and found increasing transmittance and decreasing reflectance as a function of glucose concentration [102]. The glucose-induced change has a maximum in transmittance near a wavelength of 950 nm. This maximum correlates with the high value in the absorption spectrum of water at the same wavelength range. Increasing glucose concentration decreases μ_s, but at the same time it increases the g value. [100] At lower optical scattering conditions, less light can be absorbed because the photons have a smaller probability of meeting an absorber. The effect of glucose on the optical absorption properties of tissue is mainly caused by the displacement of water by dissolved glucose molecules [100,102].

Glucose has been shown to induce larger changes in μ_s *in vivo* than *in vitro* [98]. Liu *et al*. [101] have shown that changes in the scattering properties of tissues depend not only on the change in the extracellular n. Changes in the extracellular osmolarity and cell sizes also play an important role in determining changes in the scattering properties of tissues. The effect of glucose on the scattering properties should be greater in a sample where the refractive index difference between the scattering centers and the bulk material is smaller [100].

Glucose increases the n of blood plasma. It may also induce changes in osmolarity, and hence in the shape and size of RBCs. [52] The change in the blood plasma osmolarity may induce changes in the scattering properties of blood [61,103]. Also the predisposing of RBCs to different osmotic conditions influences their shape [61,104]. The changes in their size and shape induce changes in the photons' spatial distribution and in the shape of the acoustic sound source. This is seen as a change in the PA response, i.e. pulse amplitude and pulse shape. The PA measurements show that glucose-induced changes in whole blood originate more from the changes in scattering than in absorption [66]. This was further studied also with a TOF measurement setup and a streak camera. These results show that glucose affects the arriving time of the pulse maximum and the width of the pulse [66], which are indicators for changes in scattering [105].

RBCs have been found to induce acoustic scattering (originating from mismatches between acoustic impedances) at the ultrasonic frequency of 30 MHz. [106,107] However, the frequency bandwidth of our PA measurement system was 150 kHz–3 MHz,

and acoustic scattering is significantly lower at this frequency range than at the frequency of 30 MHz. [106] Hence, the effect of ultrasound scattering may be neglected [85].

3.5 Properties of studied samples

3.5.1.1 Water

Water is the main component of the human body. Hence the absorption of water is quite dominating in many tissues over a wide range of wavelengths. In the so-called tissue optical window (wavelength range 600–1100 nm), there is an absorption minimum in the water absorption spectra (Fig. 3, [108]). For that reason, the visible and NIR spectral ranges have become very popular in biomedical diagnostics [68].

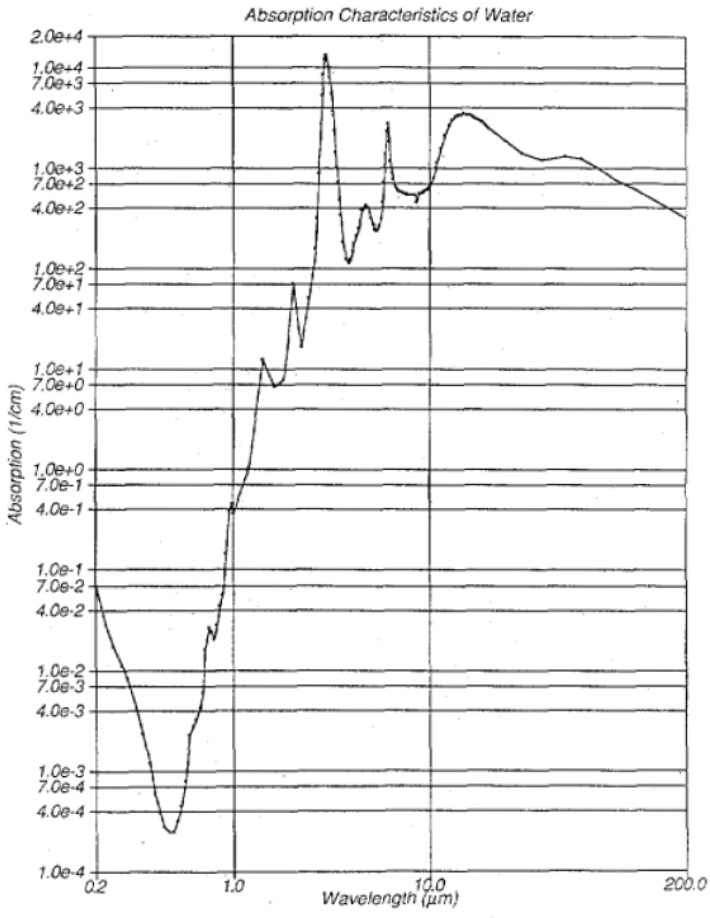

Fig. 3. Absorption spectrum of water [108]. (© [1987] IEEE)

3.5.1.2 Intralipid

10% Intralipid^{TM} (Fresenius Kabi AB, Uppsala, Sweden) was used in the measurements. Intralipid is an intravenous nutrient and it consists of phospholipid micelles and water [109]. According to the manufacturer, the constituents of Intralipid are glycerin, lecithin, soybean oil and water. The phospholipid micelles are spherical in shape and their size varies between 25–675 nm, the average size of the scattering particles being 97 ± 3 nm [110]. Intralipid is a multiple scattering, homogeneous phantom medium, and its scattering properties resemble those of skin tissue [109,111]. The n of the scattering soybean particles is about 1.46 [100,110]. The results in [112] and [113] show that the μ_s and μ_s' have nonlinear dependency as a function of Intralipid concentration. The μ_a is assumed to be the same as for water. The values for μ_s and g are shown as a function of wavelength in Fig. 4 ([110]) and Fig. 5 ([110]), respectively. The Fig. 6 ([112]) shows the μ_s' value of Intralipid as a function of concentration at a wavelength of 532 nm.

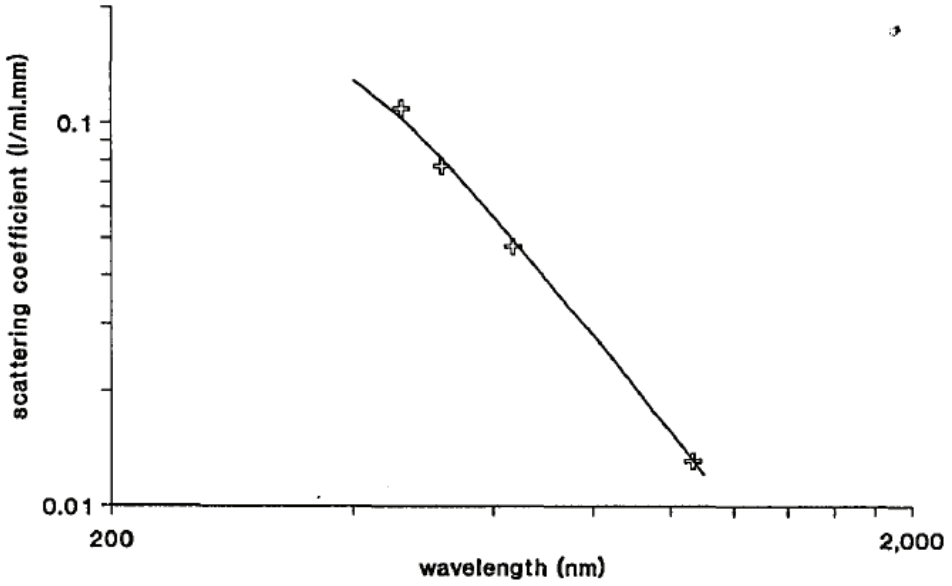

Fig. 4. Calculated scattering coefficient curve (solid line) and the experimental values (crosses) of Intralipid-10% [110]. (© [1991] Optical Society of America)

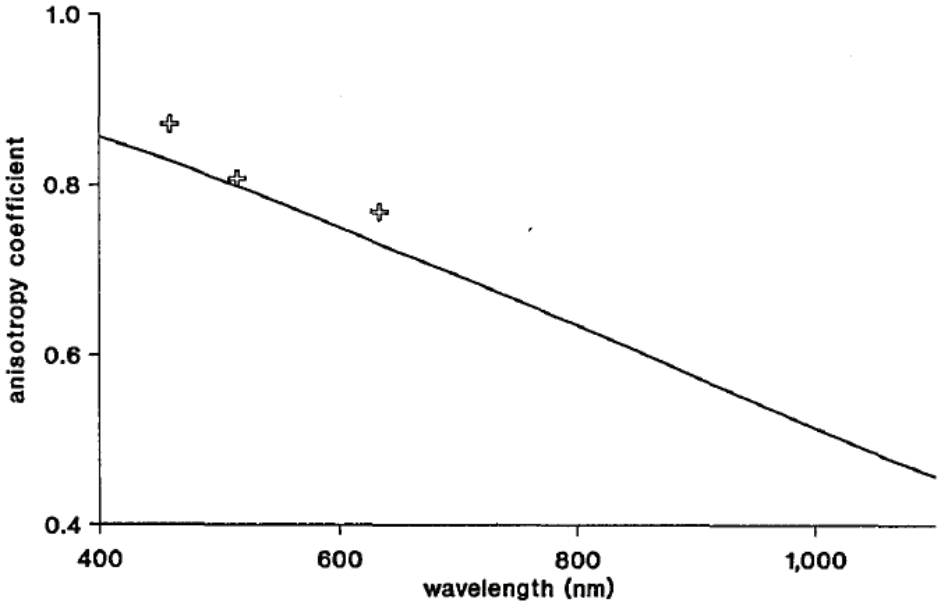

Fig. 5. Calculated anisotropy coefficient (solid line) and experimental values (crosses) of Intralipid-10% [110]. (© [1991] Optical Society of America)

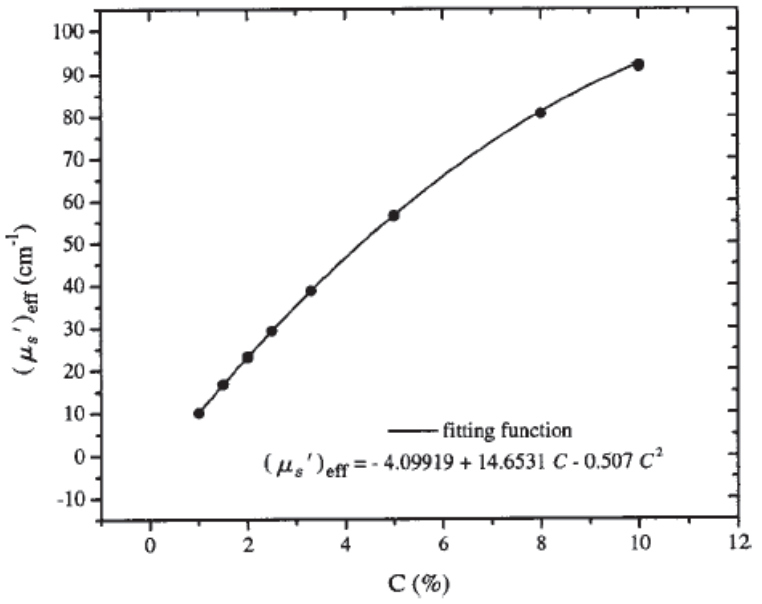

Fig. 6. Reduced scattering coefficient of Intralipid as a function of concentration at a wavelength of 532 nm [112]. (© [2003] Optical Society of America)

3.5.1.3 Blood

Blood is a vital substance circulating in the human body and in animals. Its task is, among others, to bring oxygen and nutrients to the extremities, head and various organs. Human whole blood consists of 45 vol% cells and about 55 vol% plasma. 99% of the cells are erythrocytes, and the remaining 1% are leukocytes and thrombocytes; whereas plasma consists of 90% water and 10% proteins. Red blood cells have a biconcave, flat shape and their diameter is about 7 to 8 μm. [114] Fig. 7 ([115]) shows the absorption spectrum for whole blood in the visible and NIR spectral ranges. The velocity of sound in blood is 1560 m/s [116].

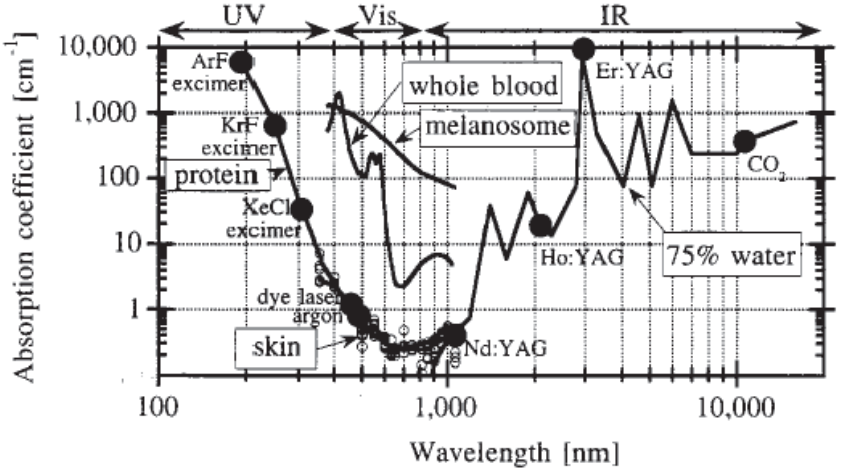

Fig. 7. Absorption spectrum of tissues [115]. (© [1996] Optical Society of America)

There are some discrepancies between human and pig blood. In pig whole blood, the size of the red blood cells varies between 4 to 8 μm, the average being 6 μm [117]. The hematocrit value of pig whole blood is lower than that of human blood. [V]

3.5.1.4 Skin tissue

Skin tissue has a layered structure, consisting of the epidermis, the dermis and subcutaneous fat. The thickness of the epidermis is typically between 75–150 μm, and that of the dermis between 2–3 mm. The epidermis consists of epithelial cells, whereas the dermis part consists of collagen fibers, elastic fibers, and an interfibrillar gel, and it contains blood vessels, lymphatic vessels and nerves. The epidermis can be subdivided into four different layers: stratum corneum, stratum granulosum, stratum spinosum, and basal cell layer, whereas two different layers can be found in the dermis: papillary and reticular dermis. The micro-vessel network is located in the papillary dermis area. [118,119]

Many different tissue components affect light scattering in skin tissue, the most effective scatterers being mitochondrias [68] and collagen fibers [119]. The absorption properties depend mainly on the oxy-hemoglobin and deoxy-hemoglobin of blood and water content in the illuminated region [103].

About 5% of the incident radiation is reflected backwards in the tissue surface due to the high n of the stratum corneum (1.55). The effect of the epidermis on the radiation is mainly attenuating because the epidermis layer is small, and the scattering is forward directed and plays a minor role. In contrast to the epidermis, the dermis layer is highly back-scattering. [119]

The thickness of mouse skin differs from that of human skin. The thickness of the epidermis and dermis are a few dozen micrometers and between 170–500 μm, respectively [120,121]. Moreover, the thickness of the dermis is greater in male than in female mice [121]. The n of mouse skin tissue is 1.40 [68].

4 Three techniques for glucose monitoring

The basics of the measurement techniques used are explained in this chapter. The OCT devices used are described in section 4.1, the PA device in section 4.2, and the TOF measurement system in section 4.3. The properties of these three techniques are briefly compared in section 4.4.

4.1 Optical coherence tomography

Optical time-domain reflectometers (OTDR) and optical low-coherence reflectometers (OLCR) are based on a Michelson interferometer and correlation detection [122]. They are able to detect scattering centers in the sample at different depths. OCT is an extension of OLCR for measuring tomographic images of tissues with a micrometer scale depth resolution, and it was first introduced by Huang *et al.* [123].

OCT uses a low coherence light source with a broad spectral bandwidth, such as a superluminescence diode (SLD) or short laser pulses with femtosecond (fs) pulse duration. The interferometer consists of the light source, an object arm and a reference arm, and a detector. The length of the reference arm is changed with a scanner, which enables the photons coming from different depths from the sample to interfere with the photons coming from the reference arm, and to generate the interference signal at the detector. The light beam has to be focused on the sample. There is a collimating and a focusing lens in the sample arm. Fig. 8 [VII] shows an example of the OCT setup.

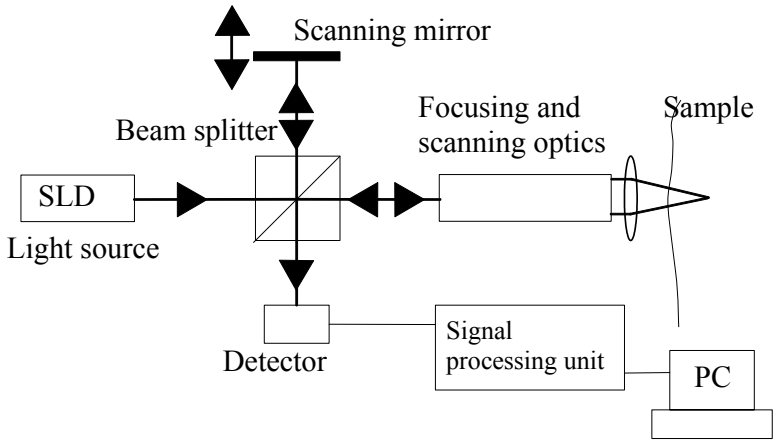

Fig. 8. Open-air optical coherence tomography system [VII].

The path length difference between the photons coming from the sample and reference arms has to be smaller than the coherence length of the light source. Thus, this detection technique mainly collects the coherently back-scattered photons. Multiple scattered photons may also reach the detector if the path length is suitable, but they distort the resolution and contrast of the OCT image. A more detailed description of the OCT can be found in Refs. [124,125] and in Papers II, III, and VI.

Different scattering-related parameters, including μ_s and g, can be extracted from the OCT signal profiles. The first approximation in determining μ_s involves utilizing the Lambert-Beer law, if $\mu_s >> \mu_a$, and μ_t is approximated by μ_s. Also the root-mean-square scattering angle (θ_{rms}) (and hence the effective anisotropy parameter g_{eff}) have been determined [126]. In addition to the mean scattering angle, Knüttel *et al*. [127] have developed a method for obtaining the n of materials. [VII]

Two different OCT devices were used in the work of this thesis. The technical specifications of the open-air system are described in Paper II, and the commercial OCT system (manufactured by the Institute of Applied Physics, Nizhny Novgorod, Russia) is described in Paper VI. The open-air system uses a wavelength of 832 nm, whereas the commercial OCT device operates at a wavelength of 910 nm. The commercial OCT system has the advantage of using a fiber optic probe with a scanner with a lateral scanning direction along the sample surface inside it. This enables the taking of 2 dimensional images of the object being studied. The depth resolution of the open-air measurement system is much better than that of the commercial OCT device. [II,VI]

4.2 Pulsed photoacoustic technique

The pulsed PA technique is based on the detection of pressure waves, generated by short laser pulses injected into the sample, with an acoustic transducer. An Nd-YAG laser with ns range pulse duration is typically used as an optical energy source. The Nd:YAG laser with 10 ns long pulses at wavelengths of 1064 nm and 532 nm (with an energy of 2 μJ

and 1 μJ, respectively) was used in the measurements. The laser pulses injected into the sample increase the temperature in the illuminated region and induce volume expansion and thus pressure waves.

Piezoelectric detectors with different film materials are typical detectors in biomedical applications. Polyvinylidenefluoride (PVDF) and lead zirconium titanate (PZT) materials are examples of polymer and ceramic film materials, respectively. Optical detection methods are also possible, but the piezoelectric ones are better in biomedical applications. [III] The position of the detector in relation to the studied object affects the measured signal. When measuring perpendicularly to the incoming laser beam in the scattering material, some photons scatter directly to the transducer. A gel can be used between the transducer and the target to improve the contact and to diminish the mismatch of acoustic impedances. Fig. 9 shows an example of a PA measurement setup for phantom measurements. The samples were put in the cuvette and the transducer was immersed into the liquid. The PA measurement setups used are described in more detail in Papers IV and V.

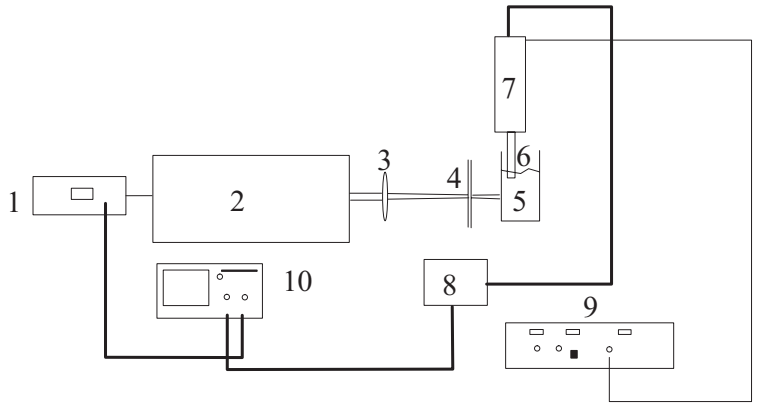

Fig. 9. Photoacoustic measurement system. 1: Laser unit, 2: Laser resonator, 3: Collimating lens, 4: Filter, 5: Cuvette, 6: Acoustic transducer, 7: Photoacoustic preamplifier, 8: Main amplifier, 9: Power unit, and 10: Oscilloscope. [V]

The PA technique enables the measurements of the optical absorption coefficient (μ_a), and sound velocity (v_a). The stress profile of the PA signal can be matched with an exponential function including parameters for the μ_a, v_a and time constant (τ_c). In turbid materials, μ_a can be replaced with μ_{eff}. To measure the optical parameters accurately, consideration of acoustic wave diffraction and attenuation is needed. [85] One recent development, the scattering photoacoustic technique (SPA), makes it possible to determine the μ_s' of the sample *in vitro* in addition to the μ_a and v_a [128,129]. [VII]

4.3 Laser pulse time-of-flight technique

In photon migration measurements with the TOF technique, short laser pulses are injected into the sample. The photons of the pulse undergo many absorption and scattering events when travelling in the sample. The scattering processes make the photon path lengths longer. Useful data can be obtained about the optical properties of the sample (μ_s and μ_a) by observing the TOF distributions of the photons and by analysing their shapes. The calculation of different pulse parameters, such as mean time-of-flight, full width at half maximum (FWHM), integral of the pulse, center-of-gravity, and moments may help in this analysis. [81,105,130, and 131] Fig. 10 shows an example of a TOF measurement system.

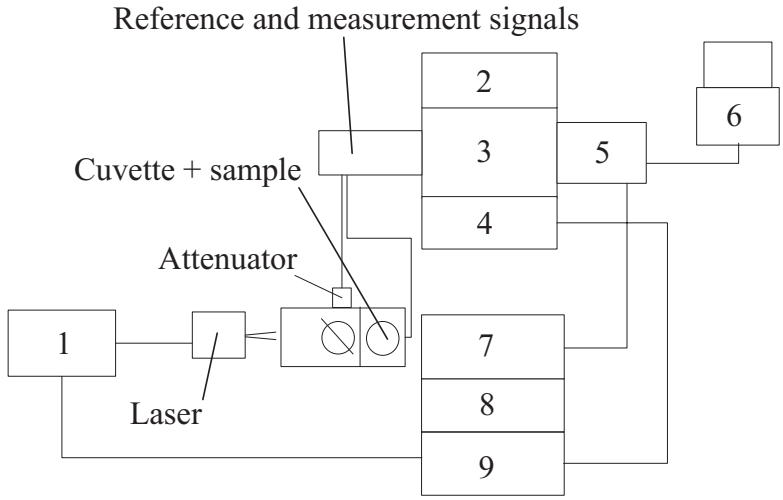

Fig. 10. Time-of-flight measurement system. 1: Picosecond laser module, 2: Blanking unit, 3: Fast speed sweep unit, 4: Streak camera, 5: Digital camera, 6: PC, 7: Camera controller, 8: Power supply unit, and 9: Delay unit.

A picosecond (ps) laser module with an approximately 30 ps pulse length at a wavelength of 906 nm was used as a light source and a streak camera was used as a detector in the laser pulse measurements. The energy of a pulse is 1 nJ. The detection of photons in the streak camera is done with a photocathode of the streak tube. The light of the photocathode is converted into electrons. The electrons travel through sweep electrodes, which direct them to the microchannel plate (MCP). The electrons are multiplied by the MCP and are eventually converted into light on a phosphor screen. The image on the phosphor screen, containing intensity information as a function of time, is captured with a CCD camera and shown on a computer screen. [132]

4.3.1 TOF measurements with optical fibers

Optical fibers are very important in modern optical measurement systems because they are flexible and facilitate the guidance of light from the light source to the sample. They enable the detection of transmitted or reflected (back-scattered) light from several points at different distances from the incident light beam simultaneously. The optical fibers also have some drawbacks, such as losses in coupling the optical power into the fiber, and induction of pulse shape distortions. The optical fibers may affect the determination of the optical properties of the sample with the TOF technique [133].

Step index (SI) fibers with 300 μm core diameters and graded index (GI) fibers with 100 μm core diameters were used in the TOF measurements. Paper I shows the figures of the measurement probes used.

4.4 Comparison of the techniques

The OCT, PA, and TOF techniques are different in origin. Each technique has its own technical parameters both for the light source and the detector, such as the operation wavelength, energy of the light source, type of light (continuous wave or pulsed), etc. These parameters have been optimized for different applications.

In TOF measurement the scattering changes are collected as an integral across the whole path length of photons. Thus, all the absorbing and scattering particles at an adequate depth in the sample affect the signal. In OCT, the signal is collected from the same point as the incident light beam. The slope value can be matched to a specific depth of the media, and therefore, the collected information is more localized. The PA technique is more sensitive than TOF and OCT in detecting strongly absorbing targets, such as blood vessels.

OCT has better spatial and depth resolutions than the PA and TOF techniques, but a smaller imaging depth. One difference between the TOF technique and the PA technique is that the PA technique has a better resolution in detecting deeper targets because the acoustic waves are not influenced by optical scattering. The PA technique can also give information directly from absorbing targets. In addition to the optical properties, the PA technique is also capable of detecting changes in thermal and acoustic parameters. Both the PA and the TOF technique can also be used to measure signals from a different side of the object than that of the incoming laser beam. The OCT and PA measurement techniques are quite quick, whereas the TOF technique with a streak camera takes a long measurement time. More comprehensive comparisons of the techniques can be found in Papers III and VII.

5 Scattering measurements with TOF, OCT, and PA techniques

This chapter presents the results achieved during the thesis work. The TOF, OCT, and PA measurement results with different Intralipid concentrations are described in sections 5.1, 5.2, and 5.3, respectively. Some of the TOF and OCT measurements are compared with MC simulations. The results in section 5.1 show the effect of glucose on the laser pulse shapes in Intralipid, the OCT measurements in section 5.2 show the effect of glucose on the OCT signal slope value in Intralipid and mouse skin tissue samples, and the results in section 5.3 show the effect of glucose on the PA signal measured in Intralipid and pig blood samples. Section 5.4 contains a more detailed discussion of the results.

5.1 TOF measurements

Photon migration measurements with the TOF technique and streak camera provide an opportunity to detect changes in the transmitted or back-scattered laser pulse shapes. The increased scattering is evident as a broadening of the pulse and delaying of the arrival time of the pulse maximum in Fig. 11 [I] when the Intralipid concentration increases. The measurements in Fig. 11 [I] were taken in a slab cuvette without optical fibers. The changes in the scattering mainly affect the rising part of the pulse. The pulse intensity decreases because the increased scattering broadens the photons' spatial and TOF distributions, resulting in fewer photons arriving at the detector, and also more photons being absorbed in the sample due to their longer traveling paths.

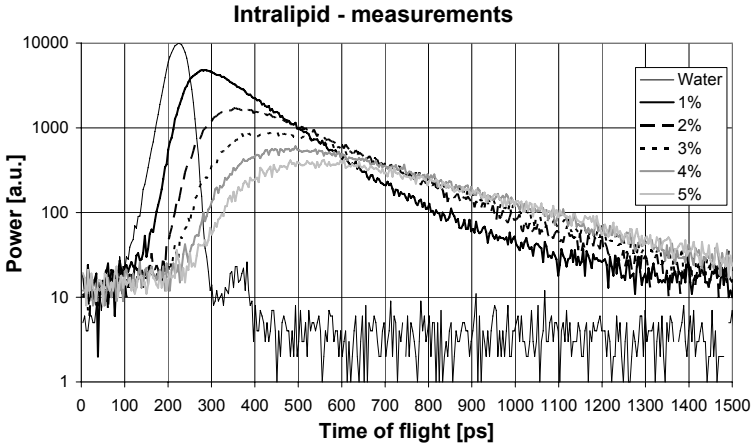

Fig. 11. Effect of Intralipid concentration on the transmitted laser pulse shapes [I].

Phantom measurements provide a rather easy way to compare theoretical models with reality. This helps in optimizing the measurement setup, and in further developing the simulation models, including into more complicated *in vitro* and *in vivo* applications. The results obtained with a MC simulation model (Fig. 12, [I]) show rather good compatibility with the measurements (Fig. 11, [I]).

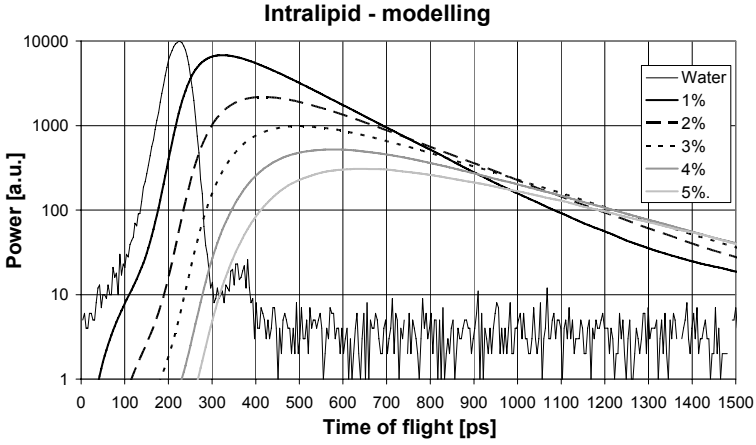

Fig. 12. Simulation results obtained with the time-of-flight technique in Intralipid phantoms [I].

The results in Paper I also show the reflectance profiles measured for different Intralipid concentrations with two different fiber-optic probes utilizing SI and GI fibers. Increasing Intralipid concentration and scattering indicates increasing back-scattering intensity.

Increasing the glucose concentration increases the transmitted pulse amplitude and shifts the pulse maximum to that of earlier times. The use of fiber-optic probes limited the optical power directed on the sample, resulting in lower sensitivity for detecting glucose-induced changes in the Intralipid phantoms than in the transmittance measurements [I]. The effect of glucose could be seen in the back-scattered pulse intensity both with SI and GI fibers when using a high glucose concentration (8,000 mg/dl). The glucose measurements also compared well with the simulations.

The results in Paper IV show that it is possible to see glucose-induced changes only in the pulse amplitude with 10 ns long pulses. This differs from the results with ps pulses, where changes can also be seen in the arrival time of the pulse maximum as well as in the pulse width when measuring transmitted laser pulses [I,IV]. The results in Fig. 13 [IV] show that the effect of glucose on the transmitted pulse amplitude in 1% Intralipid is larger at a wavelength of 1064 nm than at a wavelength of 532 nm. These results are in good comparison with the results in Ref. [100], which were measured with continuous wave light. Glucose changes the sample's scattering properties [57]. Moreover, the calculations in the Ref. [100] show that a larger relative change in transmittance can be produced at the wavelengths with high background absorption, (0.115 cm^{-1} [134] and 4.28×10^{-4} cm^{-1} [135] for water at wavelengths of 1064 nm and 532 nm, respectively), than at wavelengths with lower absorption values.

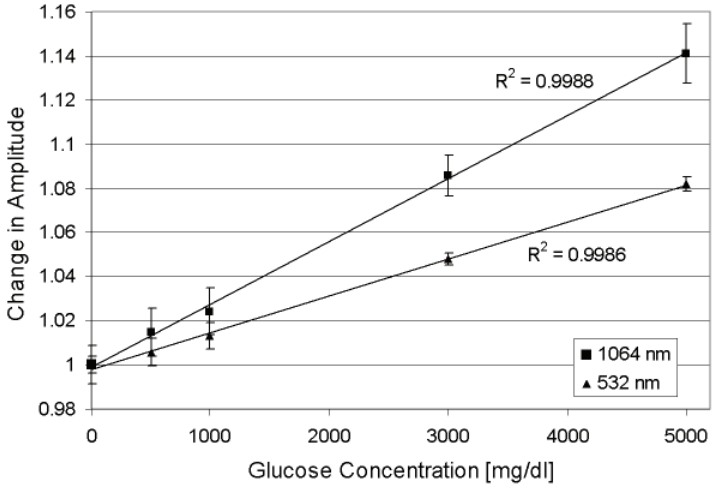

Fig. 13. Effect of glucose on the transmitted optical pulse amplitude in 1% Intralipid at wavelengths of 1064 nm and 532 nm [IV].

5.2 OCT measurements

Intralipid samples with concentrations of 2%, 5%, 7%, and 10% were measured with the open-air OCT system. These results showed large differences in the slope values between the measurements and simulations. [II]

The effect of glucose on the scattering properties was also studied. The simulations for 5% Intralipid indicate greater glucose-induced change (7% / 1,000 mg/dl) than the measurements (4.4% / 1,000 mg/dl) (Fig. 14, [II]). Moreover, the simulations show a decreasing OCT signal slope value as a function of glucose by 13% / 1,000 mg/dl [II] for 2% Intralipid. These results are discussed in greater detail in Paper II.

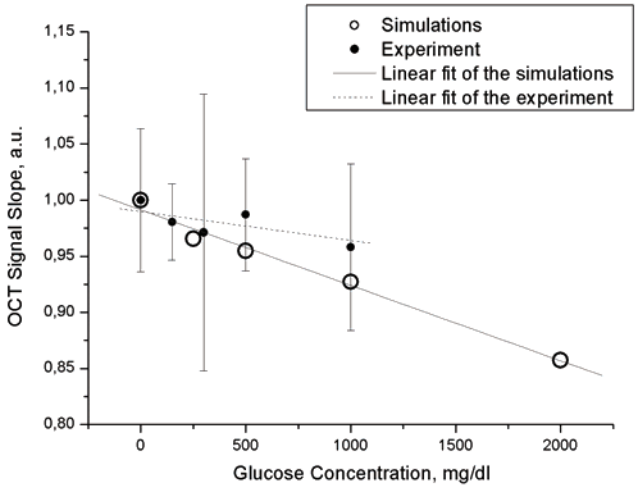

Fig. 14. Simulation and measurement results with OCT in 5% Intralipid phantom with different amounts of added glucose [II].

Due to the discrepancy between the measurements and simulations in Fig. 14 [II], the measurements were continued with another OCT device. The OCT signal depth profile can be recorded from deeper in the sample with the commercial OCT than with the open-air OCT. The increasing Intralipid concentration increases the scattering, which can be seen as increasing back-scattering intensity and an increasing OCT signal slope value (Fig. 15 (a) and (b), [VI]).

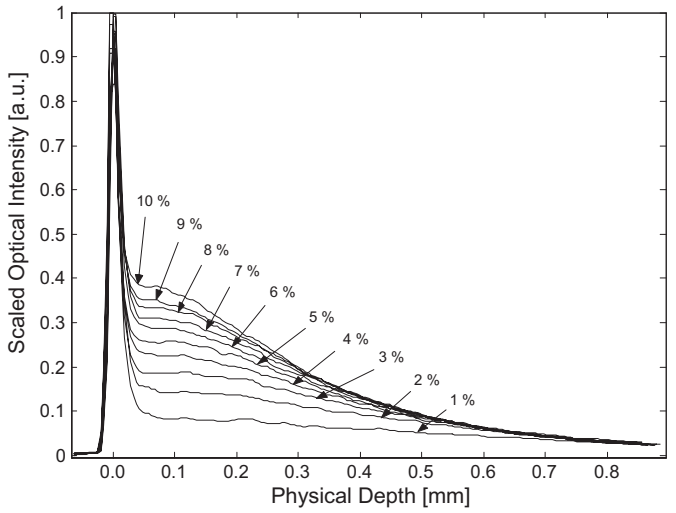

(a)

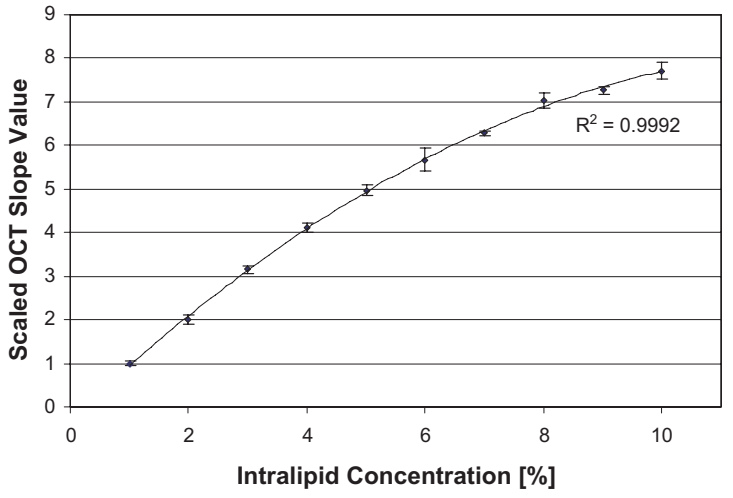

(b)

Fig. 15. OCT signal intensity profiles (a) and slope values as a function of Intralipid concentration (b) [VI].

Fig. 15 (a) [VI] demonstrates that the most pronounced effect on signal intensity is very close to the surface of the sample, and the increase is not so clear deeper in the sample. Fig. 15 (b) [VI] shows that the slope value changes nonlinearly as a function of Intralipid concentration. Quadratic fitting gives a good correlation. This change reflects the nonlinear property of μ_s and μ_s' of Intralipid [112,113]. The slope values in Fig. 15 (b) [VI] are determined from the linear fits to the profiles in Fig. 15 (a) [VI] at a depth of 0.269–0.389 mm.

The change in the slope value is different when fitting the slope at different depths. Fig. 16 shows OCT signal slope values fitted to the profiles in Fig. 15 (a) [VI] at depths of 0.192–0.336 mm and 0.625–0.769 mm. The sensitivity for detecting changes in the scattering properties is better at a depth of 0.192–0.336 mm than at 0.625–0.769 mm. In the depth range of 0.625–0.769 mm the multiple scattering and low SNR limit detection sensitivity. The coherent detection of back-scattered photons decreases the number of MSP at lower depths.

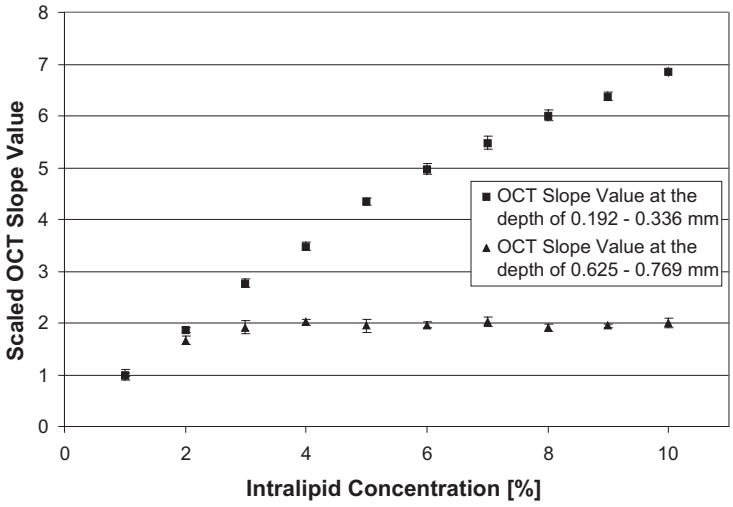

Fig. 16. Differences in the OCT signal slope values fitted to the profiles in Fig. 15 (a) at depths of 0.192–0.336 mm and 0.625–0.769 mm.

The glucose-induced decrease in the scattering can be seen as a decrease in the OCT signal slope value. Fig. 17 (a) and (b) [VI] show the results obtained from 5% and 2% Intralipid suspensions, respectively. The average glucose-induced change was found to be 1.6% / 1,000 mg/dl in 5% Intralipid and 3.9% / 1,000 mg/dl in 2% Intralipid. These values differ from the values obtained by MC simulations in Paper II. However, the change is larger in the 2% Intralipid than in the 5% Intralipid, as indicated by the simulations [II].

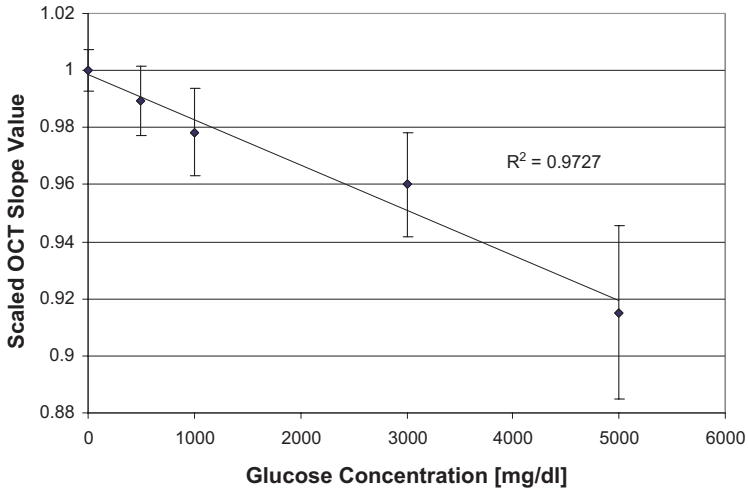

(a)

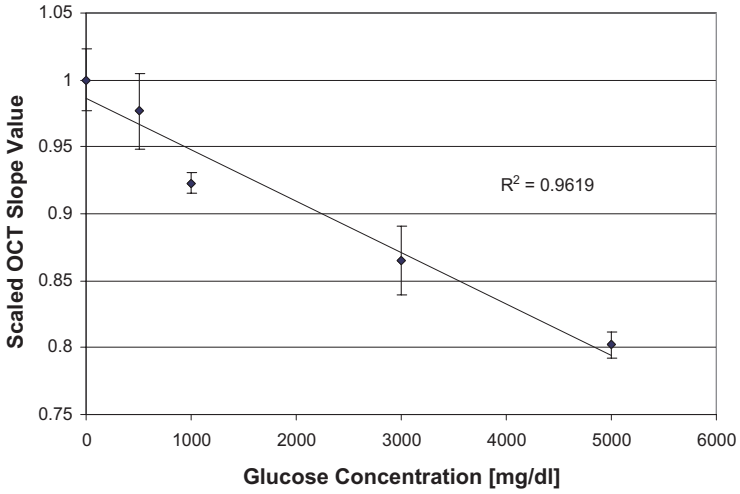

(b)

Fig. 17. Effect of glucose on the OCT signal slope value in 5% Intralipid (a) and 2% Intralipid (b) [VI].

5.2.1 Mouse skin tissue samples

Intralipid is not a very optimized model of skin [136]. Therefore, the measurement of tissue samples is a better way to study glucose-induced changes with the goal of non-invasive glucose monitoring in mind.

Mouse skin tissue samples were taken from the back of mouse embryos. The tissue samples were placed on a cell-culture dish with a nutrition media, and cultured in a CO_2 incubator before measurements. The samples were measured *in vitro* on a warming plate and in a warm room (37 ºC). Glucose concentrations were added on the dish with a pipette. The measurement procedure is described in more detail in Paper VI. The results in Fig. 18 (a) and (b) [VI] show that increasing the glucose concentration reduces the scattering properties of mouse skin tissue samples. The glucose-induced change was 0.67%/mM in Fig. 18 (a) and 1.69%/mM in Fig. 18 (b) [VI]. The standard deviation (SD) also was quite large in the measurements. Various reasons may influence the differences between the samples and the large SD, including inhomogeneities between the samples, changes in the shape and structure of the tissue specimens, and possible fluctuations in the temperature and moisture.

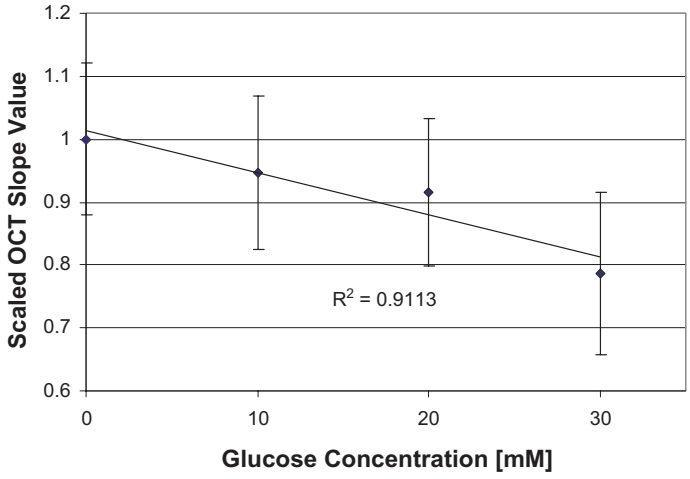

(a)

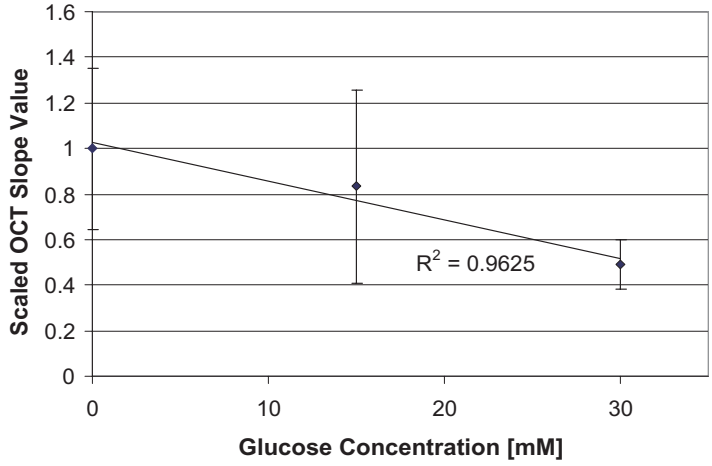

(b)

Fig. 18. Effect of glucose on the OCT signal slope value in two different mouse skin samples (a) and (b) *in vitro* [VI]. 1 mM equals 18 mg/dl, and hence the measurement range 0–30 mM equals 0–540 mg/dl.

The average change in the 5 different sets of measurements was about 1.37%/mM [VI]. The change in the scattering properties of mouse skin tissue is more pronounced than the change in Intralipid phantoms (0.07%/mM in 2% Intralipid and 0.029%/mM in 5% Intralipid, [VI]). These results show that OCT is capable of detecting much smaller changes in glucose concentrations in a biological tissue (values in a physiological range (3–30 mM)) than in the Intralipid phantom medium.

5.3 PA measurements

The increasing Intralipid concentration broadens the photons' spatial distribution and lowers the energy density in the PA sound source, which can be seen as a decreased peak-to-peak value of the PA signal. Fig. 19 [VII] shows PA signals from 1% Intralipid and 2% Intralipid suspensions. The peak-to-peak value is 14.4% lower in 2% Intralipid than in 1% Intralipid [VII].

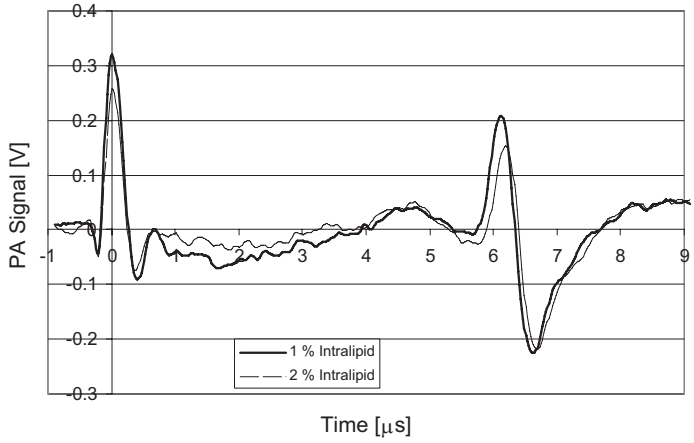

Fig. 19. Effect of Intralipid concentration on the PA signal [VII].

The first peak in Fig. 19 [VII] originates from the scattering photons hitting the PA transducer. The absorption properties of the transducer surface material and the optical properties of the sample affect the height of the first peak. The measurement geometry also has its own effect on the first peak. The bipolar waveform is produced by the PA effect in the sample.

In the PA measurements, a glucose-induced decrease in the scattering changes the photons' spatial distribution, and increases the energy density in the PA sound source. This can be seen as an increase in the peak-to-peak value of the PA signal (Fig. 20, [IV]). The glucose-induced change of 5,000 mg/dl is a little bit larger in 1% Intralipid (21.3%) than in 2% Intralipid (15.8%) [IV]. These values differ from those shown in Paper V (13.69% / 5,000 mg/dl for 1% Intralipid). Possible reasons may be different measurement distances, as well as changes in the measurement geometry. In addition to the glucose-induced changes in scattering, increasing glucose concentration also increases the sound velocity [51,65].

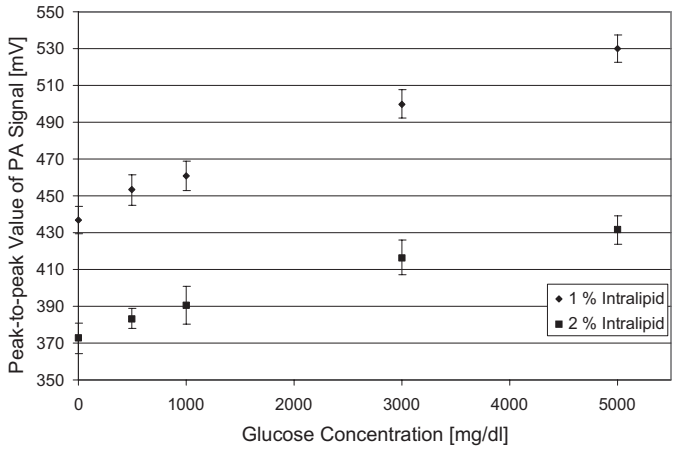

Fig. 20. Effect of glucose on the PA peak-to-peak value in 1% and 2% Intralipid suspensions [IV].

Because the absorption of Intralipid is assumed to be the same as that of water, the PA response is lower at wavelengths where the absorption of water is lower. This explains the strong and weak PA responses in Intralipid at wavelengths of 1064 nm and 532 nm, respectively [IV,V].

5.3.1 Pig blood samples

Pig whole blood was used as a sample material for studying the effects of glucose on the PA signal from blood at wavelengths of 1064 nm and 532 nm. The blood samples were poured through a cuvette using a circulating system. Due to the different optical properties of blood and Intralipid at a wavelength of 1064 nm, the shape of the acoustic sound source is more flat in blood than in Intralipid. [V]

The results in Fig. 21 [V] show that the PA signals are stronger at a wavelength of 532 nm than at 1064 nm. This is due to the higher optical absorption coefficient of blood at 532 nm. As a result, the light penetration depth is smaller at a wavelength of 532 nm.

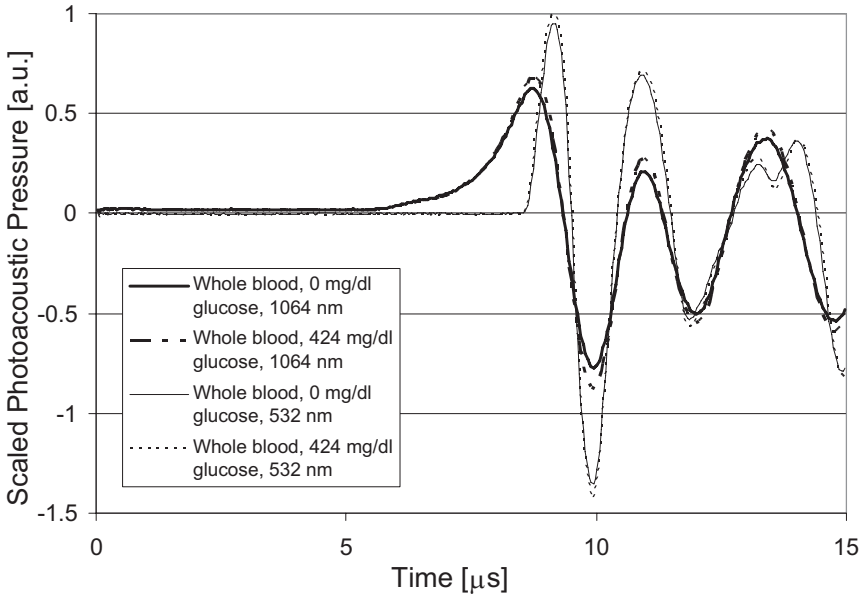

Fig. 21. The effect of glucose on the PA pulse profiles at wavelengths of 1064 nm and 532 nm. Modified from [V].

However, the measurement results show that glucose has a greater effect on the PA signal peak-to-peak value at a wavelength of 1064 nm (11.4% / 500 mg/dl, Fig. 22 (a), [V]) than at 532 nm (6.0% / 500 mg/dl, Fig. 22 (b), [V]). These values are significantly higher than the changes measured in Intralipid phantoms (Fig. 20, [IV]). The measurement results in Fig. 22 (a) and (b) were fit nicely with quadratic polynomials.

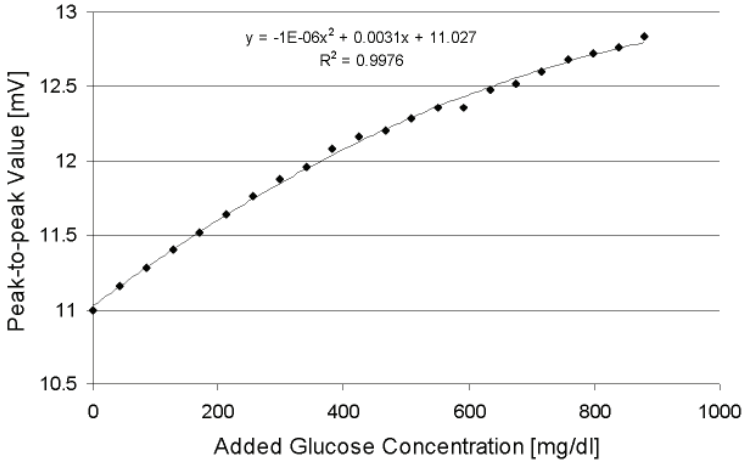

(a)

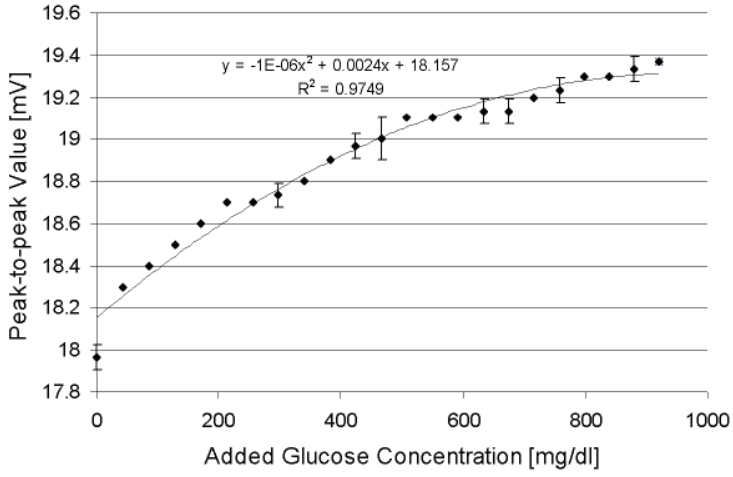

(b)

Fig. 22. The effect of glucose on the PA signal peak-to-peak value at a wavelength of 1064 nm (a) and at a wavelength of 532 nm (b) from pig whole blood [V].

5.4 Discussion of the results

The comparison of the OCT, PA, and TOF techniques shows that OCT is the most capable of detecting changes in the scattering properties of Intralipid [VII]. Each technique studied demonstrated the potentiality to detect glucose-induced changes in scattering. Although OCT can determine the changes in scattering at a specific depth, it does not specify where the changes in the scattering originate. It is also not very clear where the slope of the OCT signal profile should be fitted, and what is the optimal range for fitting. It depends on the sample being studied. When fitting the slope to detect changes in scattering, a single scattering model with an exponential attenuation is typically assumed to be valid. The use of this model results in inaccuracies when used deep in the sample. In addition, it is difficult to adjust the place of the focus of the fiber optic probe in the sample.

The PA technique needs a probe contact to the sample with piezoelectric detectors. The acoustic impedance mismatch between the sample and the transducer induces reflections of the acoustic waves, and therefore an impedance matching gel is typically used. In the liquid phantoms, the immersion of the probe into the sample makes the use of impedance matching gel unnecessary. The measurement geometry, e.g. the position of the transducer in relation to the incoming laser beam and the shape of the cuvette, affect the results. To study the low absorbing samples with higher accuracy, a more powerful laser is needed. The detection electronics also have to be improved.

The use of optical pulses with ps pulse duration makes the detection of changes in the shape of the photons' TOF distribution possible. To distinguish tiny glucose-induced changes, a more powerful laser is needed. The MC simulations in Intralipid have shown that the use of shorter laser pulses with fs pulse duration would provide the sensitivity to detect changes in the pulse amplitude and pulse area at the physiologically relevant glucose concentrations as well [137,138]. A longer measurement time with the photon-counting mode of a streak camera would improve the SNR, but it is a drawback when aiming towards *in vivo* measurements.

The Intralipid samples with different amounts of glucose were prepared as follows in Papers IV, V, and VI: First the total volume of the Intralipid needed was prepared by diluting it with distilled water. Then different amounts of glucose were added to different bottles and finally the bottles were filled up with the diluted Intralipid. The amount of scattering Intralipid particles was evaluated to decrease by 0.6% / 1,000 mg/dl, which induces a systematic error. The systematic error affects a slightly larger change in the signals than should be induced by glucose. There may also be slight variation in the Intralipid concentration between the samples, which results in small inaccuracies in the results.

Table 1 shows the glucose-induced changes in the measured signals obtained with different techniques. The effect of glucose is shown with a concentration of 1,000 mg/dl in Intralipid samples, whereas in the results from blood and skin measurements the glucose-induced changes are shown with a concentration of 500 mg/dl. Large glucose concentrations with Intralipid were used (0–5,000 mg/dl) because the effect of glucose on the scattering properties of Intralipid is very weak. The results in Fig. 22 [V] and Fig. 18 [VI], and in *Table 1* show that the effect of glucose on the scattering properties of

biological materials are much larger than on the scattering properties of Intralipid, and hence changes in the physiological range (about 18–450 mg/dl) are also detectable.

Table 1. Comparison of the glucose-induced changes in the measured signals.

Measured signal parameter	λ (nm)	Intralipid*			Blood**	Skin**
		1%	2%	5%		
OCT, slope value	832			4.4% [II]		
	910		3.9% [VI]	1.6% [VI]		38% [VI]
PA, peak-to-peak value	1064	5.5% [IV]	4.7% [IV]		11.4% [V]	
		2.7% [V]				
PA, peak-to-peak value	532				6% [V]	
TOF, pulse amplitude	906		5.8% [I]			
			> 30% [IV]			
TOF, pulse width	906		-1.3% [I]			
			-12% [IV]			
TOF, pulse arriving time	906		-1.1% [I]			
			-25.6% [IV]			

*Glucose concentration = 1,000 mg/dl. **Glucose concentration = 500 mg/dl.

The Intralipid measurements with the TOF technique show changes in the pulse amplitude, the pulse width, and in the arrival time of the pulse maximum. Changes in the profile can also be seen with high glucose concentrations [I,IV]. The possible reasons for different results in Papers I and IV may be in the use of the cuvettes with different shapes and in the use of optical fibers to guide the transmitted light from the cuvette to the streak camera in Paper IV. However, the use of optical fibers in IV had the advantage of measuring the reference pulse at the same time, which makes it easier to correct the walking error of the measurement device. The Intralipid measurement results obtained with different techniques are compared in Paper VII.

The glucose measurements with OCT show that the effect of glucose is in the same range in the Intralipid phantoms (0.07 and 0.029%/mM for 2% and 5% Intralipid respectively) as in polystyrene microsphere suspension (0.023%/mM) and in 3% fat milk (0.032%/mM) [59].

The measurement results from 5% Intralipid (Fig. 23 (a) and (b)) show that the specificity of the OCT technique in glucose measurements is poor deep in the Intralipid phantom due to the low SNR and the MSPs. A clear trend can be found in the slope values as a function of glucose in the A range, but not in the B range (Fig. 23 (b)). The SD is greater in the B range than in the A range at every different glucose concentration.

The measurements of mouse skin tissue samples at a wavelength of 910 nm show larger glucose-induced change in the slope value (0.67–1.74%/mM) than the Intralipid measurements, whereas the effect in these samples is smaller than in the *in vivo* animal studies at a wavelength of 1300 nm [12]. Possible reasons for the difference between the results from Intralipid and skin tissue samples may be the different sizes and shapes of the scattering particles, as well as their refractive indices. In the mouse skin samples, there was no blood in the samples in the *in vitro* measurements, and scattering was mainly induced by mitochondria [68],[VI].

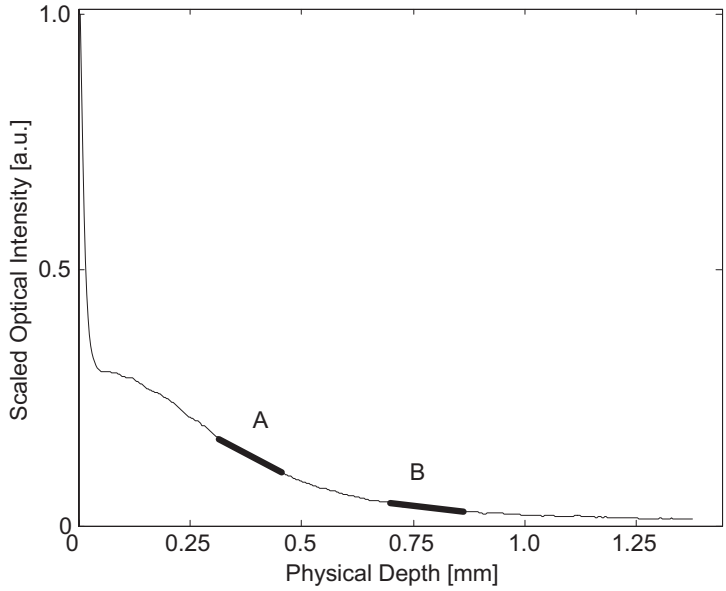

(a)

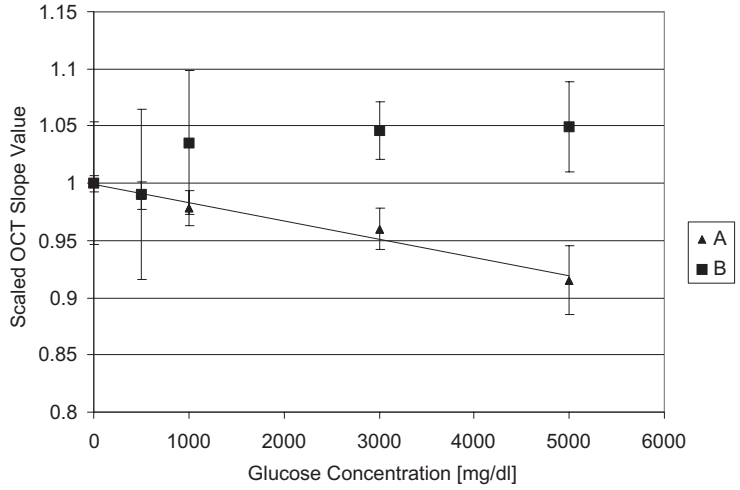

(b)

Fig. 23. The effect of depth on slope determination. (a) Depth profile from 5% Intralipid, and (b) the slope values fitted to the A and B ranges in Fig. 23 (a).

The PA measurements show varying results in 1% Intralipid (2.7 and 5.5% / 1,000 mg/dl) and a change of 4.7% / 1,000 mg/dl in 2% Intralipid. These results highlight the importance of the stabilization of the measurement conditions. However, these are in the same range as the results obtained from 3% fat milk (5.4%) [51].

The different values for glucose-induced changes in 1% and 2% Intralipid with the PA technique and in 2% and 5% Intralipid with OCT can be explained by the fact that when the initial scattering and the mean refractive index are higher, more glucose is needed to achieve the same effect in the registered signal as in a low-scattering case.

The PA measurement results in blood in Ref. [63] show a 7% increase in the peak-to-peak value when glucose increases from 88 mg/dl to 500 mg/dl at a wavelength of 905 nm. The corresponding increase in Fig. 22 [V] shows an increase of 10.2% at a wavelength of 1064 nm and 5.3% at a wavelength of 532 nm, which are good in comparison to Ref. [63]. The glucose-induced change is clearly dependent on the wavelength, and it is much greater in blood than in Intralipid. The possible reason for different glucose-induced changes in blood and in Intralipid may originate from different refractive indices of the scattering particles, but also from the possible changes in the shapes of red blood cells [V].

Temperature is an important factor which may affect the sample's optical parameters in non-invasive glucose monitoring *in vitro*. Increasing temperature has been shown to decrease scattering. [57] In Intralipid measurements, the stabilizing of room and sample temperature ensures better results. Several other parameters have to be taken into account when measuring biological samples such as blood and skin. These include e.g. variation in humidity, pH-level, and the CO_2 level in skin tissue measurements and blood oxygenation in blood measurements [V,VI]. Possible problems in glucose measurements *in vivo* are discussed in Paper III.

The results of this thesis show that although OCT, PA, and TOF techniques are capable of detecting glucose-induced changes in different samples, no method was found which would make invasive calibration unnecessary by combining different techniques. This problem needs to be studied further in the future, and could possibly be approached by measuring glucose-induced changes in a sample using several methods simultaneously.

5.4.1 Future work

Optical measurement techniques are developing continuously. Even during the time period of this thesis project, the number of measurement devices in our laboratory increased. Moreover, new measurements with biological samples are possible. Future studies include *in vivo* glucose monitoring with OCT from mice. This is the next step following the measurements conducted in Paper VI.

The sensitivity of the PA and TOF techniques will be improved with a more energetic laser source in the PA technique, and with a pulsed Ti-Sapphire laser with fs pulse duration in the TOF technique. The Intralipid measurements with the TOF technique will be continued with a fiber-optic probe with GI fibers with core diameters of 300 μm.

6 Summary

This thesis reviewed the relevant literature concerning non-invasive glucose monitoring techniques. Three techniques, optical coherence tomography, the pulsed photoacoustic technique and the time-of-flight technique were studied in greater detail. Intralipid was used as a tissue-simulating phantom to compare these techniques. In addition, glucose-induced changes in the optical properties of Intralipid were measured with these techniques. For biological samples, pig whole blood was used in the PA measurements and mouse skin tissue in the OCT measurements. All the measurements were taken in *in vitro* conditions.

Increasing the Intralipid concentration has the following effects on the signals measured: 1) the number of back-scattering photons increases and the OCT signal intensity increases, 2) the mean flight time of photons through the sample and the width of the transmitted pulse increases and the pulse intensity decreases, 3) the shape of the photons' spatial distribution change, and hence the energy density in the sample (and in the PA sound source) decreases and the peak-to-peak value of the detected PA signal decreases.

Increasing the glucose concentration increases the refractive index of the Intralipid bulk material, and hence the refractive index mismatch between the scattering centers and the bulk material decreases. This results in the following changes in the signals: 1) The OCT signal slope value decreases; 2) The detected TOF distribution becomes narrower, and the number of earlier arriving photons increases. The decrease in scattering mostly affects the rising part of the pulse. The travelling speed of light decreases too. 3) The decreased scattering changes the shape of the photons' spatial distribution, increases the energy density in the PA sound source, and also the peak-to-peak value of the PA signal. The increasing glucose concentration also displaces water in the sample and slightly affects its absorption properties and sound velocity.

The glucose-induced changes in the signals measured from Intralipid depend on the measurement setup and the technique. The signal processing has its own effects too. The effect of 1,000 mg/dl glucose on 2% Intralipid was recorded as inducing a 3.9% change in the OCT signal slope value, a 4.7% change in the PA signal peak-to-peak value and a 5.8% change in the TOF pulse amplitude. In the OCT measurements, the effect of glucose

was larger in 2% than in 5% Intralipid, and in the PA measurements, the effect of glucose was larger in 1% than in 2% Intralipid.

The effect of glucose on the peak-to-peak value of the PA signal in blood was recorded to be 6.0% / 500 mg/dl at a wavelength of 532 nm and 11.4% / 500 mg/dl at a wavelength of 1064 nm, and on the OCT signal slope value 1.37%/mM (38%/500 mg/dl) in a mouse skin tissue sample at a wavelength of 910 nm. The wavelength affects the changes detected with the PA technique. The PA technique is good for measuring blood due to the high optical absorption of blood, whereas OCT is more suitable for measuring changes in the scattering properties directly.

OCT is a good tool for medical imaging of, e.g. skin and eye tissues, due to its high depth and axial resolutions. It is a potential technique for non-invasive glucose monitoring because of its ability to detect glucose-induced changes in the scattering properties in different layers of the sample. The problems in glucose monitoring arise from the indirect nature of the measurements because OCT is not specific for single glucose molecules. Only relative changes can be found when analysing the interference signal. The PA technique is good for imaging absorbing targets due to the photoacoustic effect. The TOF technique has the ability to detect changes both in absorption and in the scattering properties of the sample by analysing the detected laser pulse shapes. The long measurement time with a streak camera restricts the applicability of the TOF technique for continuous non-invasive glucose monitoring.

In conclusion, it is not possible to detect the accurate glucose level with the OCT, PA, and TOF techniques, although each technique shows changes in the signals in *in vitro* measurements, at least with high glucose concentrations. All these techniques are dependent on invasive calibration. OCT is the most sensitive of these three techniques in detecting changes in the scattering properties of Intralipid. The *in vitro* measurements with OCT at a wavelength of 910 nm show that the effect of glucose on the scattering properties of cultured mouse skin tissue samples is greater than on the scattering properties of an Intralipid phantom. The PA measurements show that although the PA pulses are stronger at a wavelength of 532 nm, the glucose-induced change in the pig whole blood is greater at a wavelength of 1064 nm than at 532 nm. The detection of optical pulses showed that glucose-induced changes were larger in the transmitted pulse amplitude in a 1% Intralipid phantom at a wavelength of 1064 nm than at a wavelength of 532 nm. The duration of nanosecond range optical pulses was too long to distinguish small glucose-induced changes in the detected temporal TOF distribution of photons. The TOF measurements with picosecond laser pulses and a streak camera were only taken in the Intralipid phantoms. These results show that glucose mainly affects the rising part of the pulse.

References

1. Atkinson MA & Maclaren NK (1994) The pathogenesis of insulin-dependent diabetes mellitus. The New England Journal of Medicine 331: 1428–1436.
2. Amos AF, McCarty DJ & Zimmet P (1997) The rising global burden of diabetes and its complications: estimates and projections to the year 2010. Diabetic Medicine 14: S7–S85.
3. King H, Aubert RE & Herman WH (1998) Global burden of diabetes, 1995–2025. Prevalence, numerical estimates, and projections. Diabetes Care 21: 1414–1431.
4. Page SR & Peacock I (1993) Blood glucose monitoring: does technology help? Diabetic Medicine 10: 793–801.
5. Wilkins E & Atanasov P (1996) Glucose monitoring: state of the art and future possibilities. Medical Engineering & Physics 18: 273–288.
6. Ginsberg BH (1992) An overview of minimally invasive technologies. Clinical Chemistry 38: 1596–1600.
7. Wilson GS, Zhang Y, Reach G, Moatti-Sirat D, Poitout V, Thévenot DR, Lemonnier F & Klein J-C (1992) Progress toward the development of an implantable sensor for glucose. Clinical Chemistry 38: 1613–1617.
8. Leboulanger B, Guy RH & Delgado-Charro MB (2004) Reverse iontophoresis for non-invasive transdermal monitoring. Physiological Measurement 25: R35–R50.
9. Klonoff DC (2005) Continuous glucose monitoring, roadmap for 21st century diabetes therapy. Diabetes Care 28: 1231–1239.
10. Pickup JC, Hussain F, Evans ND & Sachedina N (2005) In vivo glucose monitoring: the clinical reality and the promise. Biosensors and Bioelectronics 20: 1897–1902.
11. DCCT Research Group (1993) The effect of intensive treatment of diabetes on the development and progression of long-term complications in insulin-dependent diabetes mellitus. The New England Journal of Medicine 329: 977–986.
12. Larin KV, Motamedi M, Ashitkov TV & Esenaliev RO (2003) Specificity of non-invasive blood glucose sensing using optical coherence tomography technique: a pilot study. Physics in Medicine and Biology 48: 1371–1390.
13. Voet D & Voet JG (1995) Biochemistry. Second edition, John Wiley & Sons Inc., New York, USA.
14. Zierler K (1999) Whole body glucose metabolism. American Journal of Physiology 276 (Endocrinology and Metabolism 39): E409–E426.

15. Stahl M, Brandslund I, Jørgensen LGM, Hyltoft Petersen P, Borch-Johnsen K & de Fine Olivarius N (2002) Can capillary whole blood glucose and venous plasma glucose measurements be used interchangeably in diagnosis of diabetes mellitus. Scandinavian Journal of Clinical & Laboratory Investigation 62: 159–166.
16. Bruulsema JT, Hayward JE, Farrell TJ, Patterson MS, Heinemann L, Berger M, Koschinsky T, Sandahl-Christiansen J, Orskov H, Essenpreis M, Schmelzeisen-Redeker G & Böcker D (1997) Correlation between blood glucose concentration in diabetics and non-invasively measured tissue optical scattering coefficient. Optics Letters 22: 190–192.
17. Heinemann L & Schmelzeisen-Redeker G (1998) Non-invasive continuous glucose monitoring in Type 1 diabetic patients with optical glucose sensors. Diabetologia 41: 848–854.
18. Heise KM (1996) Non-invasive monitoring of metabolites using near infrared spectroscopy: state of the art. Hormones Metabolism Research 28: 527–534.
19. Coté GL (1997) Non-invasive optical glucose sensing – an overview. Journal of Clinical Engineering 22: 253–259.
20. Waynant RW & Chenault VM (1998) Overview of non-invasive fluid glucose measurement using optical techniques to maintain glucose control in diabetes mellitus. LEOS Newsletter 4: 3–6.
21. Khalil OS (1999) Spectroscopic and clinical aspects of non-invasive glucose measurements. Clinical Chemistry 45: 165–177.
22. Khalil OS (2004) Non-invasive glucose measurement technologies: an update from 1999 to the dawn of the new millennium. Diabetes Technology & Therapeutics, 6: 660–697.
23. McNichols RJ & Coté GL (2000) Optical glucose sensing in biological fluids: an overview. Journal of Biomedical Optics 5: 5–16.
24. Malin SF, Ruchti TL, Blank TB, Thennadil SN & Monfre SL (1999) Non-invasive prediction of glucose by near infrared diffuse reflectance spectroscopy. Clinical Chemistry 45: 1651–1658.
25. Marbach R, Koschinsky TH, Gries FA & Heise HM (1993) Non-invasive blood glucose assay by near-infrared diffuse reflectance spectroscopy of the human inner lip. Applied Spectroscopy 47: 875–881.
26. Arnold MA (1996) Non-invasive glucose monitoring. Current Opinion in Biotechnology 7: 46–49.
27. Maruo K, Tsurugi M, Chin J, Ota T, Arimoto H, Yamada Y, Tamura M, Ishii M & Ozaki Y (2003) Non-invasive blood glucose assay using a newly developed near-infrared system. IEEE Journal of Selected Topics in Quantum Electronics 9: 322–330.
28. Liu R, Chen W, Gu X, Luo Y & Xu K (2005) Extraction of glucose information in blood glucose measurement by non-invasive near-infrared spectra. Proceedings of SPIE 5702: 30–38.
29. Zeller H, Novak P & Landgraf R (1989) Blood glucose measurement by infrared spectroscopy. The International Journal of Artificial Organs 12: 129–135.
30. Mendelson Y, Clermont AC, Peura RA & Lin B-C (1990) Blood glucose measurement by multiple attenuated total reflection and infrared absorption spectroscopy. IEEE Transactions on Biomedical Engineering 37: 458–465.
31. Klonoff DC, Braig J, Sterling B, Kramer C, Goldberger D & Trebino R (1998) Mid-infrared spectroscopy for non-invasive blood glucose monitoring. IEEE Laser Electro-Optics Society Newsletter 12: 13–14.

32. Bruulsema JT, Essenpreis M, Heinemann L, Hayward JE, Berger M, Gries FA, Koschinsky T, Sandahl-Christiansen J, Orskov H, Farrell TJ, Patterson MS & Böcker D (1996) Detection of changes in blood glucose concentration in vivo with spatially resolved diffuse reflectance. OSA TOPS on Biomedical Optical Spectroscopy and Diagnostics 3: 2–6.
33. Heinemann L, Krämer U, Klötzer H-M, Hein M, Volz D, Hermann M, Heise T & Rave K (2000) Non-invasive glucose measurement by monitoring scattering coefficient during oral glucose tolerance test. Diabetes Technology & Therapeutics 2: 211–220.
34. Khalil OS, Yeh S-j, Lowery MG, Wu X, Hanna CF, Kantor S, Jeng T-W, Kanger JS, Bolt RA & de Mul FF (2003) Temperature modulation of the visible and near infrared absorption and scattering coefficients of human skin. Journal of Biomedical Optics 8: 191–205.
35. Yeh S-j, Khalil OS, Hanna CF & Kantor S (2003) Near-infrared thermo-optical response of the localized reflectance of intact diabetic and non-diabetic human skin. Journal of Biomedical Optics 8: 534–544.
36. McNichols RJ, Cameron BD & Coté GL (1998) Development of a non-invasive polarimetric glucose sensor. LEOS Newsletter 4: 30–31.
37. Chou C, Han C-Y, Kuo W-C, Huang Y-C, Feng C-M & Shyu J-C (1998) Non-invasive glucose monitoring in vivo with an optical heterodyne polarimeter. Applied Optics 37: 3553–3557.
38. Ansari RR, Böckle S & Rovati L (2004) New optical scheme for a polarimetric-based glucose sensor. Journal of Biomedical Optics 9: 103–115.
39. Lambert J, Storrie-Lombardi M & Borchert M (1998) Measurement of physiological glucose levels using Raman spectroscopy in a rabbit aqueous humor model. LEOS Newsletter 4: 19–22.
40. Berger AJ, Wang Y & Feld MS (1996) Rapid, non-invasive concentration measurements of aqueous biological analytes by near-infrared Raman spectroscopy. Applied Optics 35: 209–212.
41. Berger AJ, Koo T-W, Itzkan I, Horowitz G & Feld MS (1999) Multicomponent blood analysis by near-infrared Raman spectroscopy. Applied Optics 38: 2916–2926.
42. Goetz MJ, Coté GL, Erckens R, March W & Motamedi M (1995) Application of a multivariate technique to Raman spectra for quantification of body chemicals. IEEE Transactions on Biomedical Engineering 42: 728–731.
43. Enejder AMK, Scecina TG, Oh J, Hunter M, Shih W-C, Sasic S, Horowitz GL & Feld MS (2005) Raman spectroscopy for non-invasive glucose measurements. Journal of Biomedical Optics 10: 031114 (1–9).
44. Pickup JC, Hussain F, Evans ND, Rolinski OJ & Birch DJS (2005) Fluorescence-based glucose sensors. Biosensors and Bioelectronics 20: 2555–2565.
45. Rosencwaig A (1980) Photoacoustics and Photoacoustic Spectroscopy. John Wiley & Sons Inc., New York, Chischester, Brisbane, Toronto.
46. Tam AC (1986) Applications of photoacoustic sensing techniques. Reviews of Modern Physics 58: 381–431.
47. Christison GB & MacKenzie HA (1993) Laser photoacoustic determination of physiological glucose concentrations in human whole blood. Medical & Biological Engineering & Computing 31: 284–290.
48. Quan KM, Christison GB, MacKenzie HA & Hodgson P (1993) Glucose determination by a pulsed photoacoustic technique: an experimental study using a gelatin-based tissue phatom. Physics in Medicine and Biology 38: 1911–1922.

49. MacKenzie HA, Ashton HS, Spiers S, Shen Y, Freeborn SS, Hannigan J, Lindberg J & Rae P (1999) Advances in photoacoustic non-invasive glucose testing. Clinical Chemistry 45: 1587–1595.
50. Ashton HS, MacKenzie HA, Rae P, Shen YC, Spiers S & Lindberg J (1999) Blood glucose measurements by photoacoustics. CP463 Photoacoustic and Photothermal Phenomena: 10th International Conference: 570–572.
51. Zhao Z (2002) Pulsed photoacoustic techniques and glucose determination in human blood and tissue. Dissertation, University of Oulu, Finland.
52. Bednov AA, Savateeva EV & Oraevsky AA (2003) Glucose monitoring in whole blood by measuring laser-induced acoustic profiles. Proceedings of SPIE 4960: 21–29.
53. Esenaliev RO, Larin KV & Larina IV (2001) Non-invasive monitoring of glucose concentration with optical coherence tomography. Optics Letters 26: 992–994.
54. Larin KV, Larina I, Motamedi M, Gelikonov V, Kuranov R & Esenaliev R (2001) Potential application of optical coherence tomography for non-invasive monitoring of glucose concentration. Proceedings of SPIE 4263: 83–90.
55. Larin KV, Motamedi M, Eledrisi MS & Esenaliev RO (2002) Non-invasive blood glucose monitoring with optical coherence tomography, a pilot study in human subjects. Diabetes Care 25: 2263–2267.
56. Larin KV (2002) Measurement of tissue optical properties with optical coherence tomography: implication for non-invasive blood glucose concentration monitoring. Dissertation, the University of Texas Medical Branch at Galveston.
57. Chance B, Liu H, Kitai T & Zhang Y (1995) Effects of solutes on optical properties of biological materials: models, cells, and tissues. Analytical Biochemistry 227: 351–362.
58. Larin KV, Ashitkov TV, Larina IV, Petrova IY, Eledrisi M, Motamedi M & Esenaliev RO (2002) Optical coherence tomography technique for non-invasive blood glucose monitoring: phantom, animal and human studies. Proceedings of SPIE 4619: 157–164.
59. Larin KV, Ashitkov TV, Larina I, Petrova I, Eledrisi M, Motamedi M & Esenaliev RO (2004) Optical coherence tomography and non-invasive blood glucose monitoring: a review. Proceedings of SPIE 5474: 285–290.
60. Zhao Z & Myllylä R (2001) The scattering effect of glucose on near-infrared photoacoustic detection sensitivity in tissue measurements. Asian Journal of Physics 10.
61. Tuchin VV, Xu X & Wang RK (2002) Dynamic optical coherence tomography in studies of optical clearing, sedimentation, and aggregation of immersed blood. Applied Optics 41: 258–271.
62. Tuchin VV (2005) Optical clearing of tissues and blood using the immersion method. Journal of Physics D: Applied Physics 38: 2497–2518.
63. Zhao Z & Myllylä R (2001) Photoacoustic determination of glucose concentration in whole blood by near-infrared laser diode. Proceedings of SPIE 4256: 77–83.
64. MacKenzie HA, Christison GB, Hodgson P & Blanc D (1993) A laser photoacoustic sensor for analyte detection in aqueous systems. Sensors and Actuators B 11: 213–220.
65. Shen Y, Lu Z, Spiers S, MacKenzie HA, Ashton HS, Hannigan J, Freeborn SS & Lindberg J (2000) Measurement of the optical absorption coefficient of a liquid by use of a time-resolved photoacoustic technique. Applied Optics 39: 4007–4012.
66. Zhao Z & Myllylä R (2002) Photoacoustic blood glucose and skin measurement based on optical scattering effect. Proceedings of SPIE 4707: 153–157.

67. Cubeddu R, Pifferi A, Taroni P, Torricelli A & Valentini G (1997) A solid tissue phantom for photon migration studies. Physics in Medicine and Biology 42: 1971–1979.
68. Tuchin VV (2000) Tissue Optics: Light Scattering Methods and Instruments for Medical Diagnosis. Tutorial texts in optical engineering, Vol. TT38. SPIE PRESS, Bellingham, Washington, USA.
69. Alonso M & Finn EJ (1967) Fundamental university physics. Vol. 2. Addison-Wesley Publishing Company, USA
70. Ishimaru A (1978) Wave Propagation and Scattering in Random Media. Vol. 1, Academic Press, New York.
71. Tuchin VV (Editor) (1994) Selected Papers on Tissue Optics, Application in Medical Diagnosis and Therapy. SPIE Milestone Series, MS 102, Bellingham, USA.
72. Cheong W-F, Prahl SA & Welch AJ (1990) A review of the optical properties of biological tissues. IEEE Journal of Quantum Electronics 26: 2166–2185.
73. Patterson MS, Chance B & Wilson BC (1989) Time-resolved reflectance and transmittance for the non-invasive measurement of tissue optical properties. Applied Optics 28: 2331–2336.
74. Jacques SL (1989) Time-resolved reflectance spectroscopy in turbid tissues. IEEE Transactions on Biomedical Engineering 36: 1155–1161.
75. Wilson BC & Adam G (1983) A Monte Carlo model for the absorption and flux distributions of light in tissue. Medical Physics 10: 824–830.
76. Karabutov AA, Pelivanov IM, Podymova NB & Skipetrov SE (1999) Direct measurement of the spatial distribution of light intensity in a scattering medium. JETP Letters 70: 183–188.
77. Karabutov AA, Pelivanov IM, Podymova NB & Skipetrov SE (1999) Determination of the optical charasteristics of turbid media by the laser optoacoustic method. Quantum Electronics 29: 1054–1059.
78. Grashin PS, Karabutov AA, Oraevsky AA, Pelivanov IM, Podymova NB, Savateeva EV & Solomatin VS (2002) Distribution of the laser radiation intensity in turbid media: Monte Carlo simulations, theoretical analysis, and results of optoacoustic measurements. Quantum Electronics 32: 868–874.
79. Nilsson AMK, Berg R & Andersson-Engels S (1995) Measurements of the optical properties of tissue in conjunction with photodynamic therapy. Applied Optics 34: 4609–4619.
80. Tsai C-L, Yang Y-F, Han C-C, Hsieh J-H & Chang M (2001) Measurement and simulation of light distribution in biological tissues. Applied Optics 40: 5770–5777.
81. Yoo KM, Das BB, Liu F & Alfano RR (1993) Ultrashort laser pulse propagation and imaging in biological tissue and model random media – steps towards optical mammography. SPIE Medical Optical Tomography: Functional Imaging and Monitoring IS11: 425–449.
82. Podgaetsky VM, Tereshchenko SA, Smirnov AV & Vorob'ev NS (2000) Bimodal temporal distribution of photons in ultrashort laser pulse passed through a turbid medium. Optics Communications 180: 217–223.
83. Diebold GJ & Sun T (1994) Properties of photoacoustic waves in one, two, and three dimensions. Acustica 80: 339–351.
84. Zhao Z, Nissilä S, Ahola O & Myllylä R (1998) Production and detection theory of pulsed photoacoustic wave with maximum amplitude and minimum distortion in absorbing liquid. IEEE Transactions on Instrumentation and Measurements 47: 578–583.

85. Oraevsky AA, Jacques SL & Tittel FK (1997) Measurement of tissue optical properties by time-resolved detection of laser-induced transient stress. Applied Optics 36: 402–415.
86. Zhao Z & Myllylä R (2001) The effects of optical scattering on pulsed photoacoustic measurement in weakly absorbing liquids. Measurement Science and Technology 12: 2172–2177.
87. Sigrist MW (1986) Laser generation of acoustic waves in liquids and gases. Journal of Applied Physics 60: R83–R121.
88. Terzic M & Sigrist MW (1984) Diffraction characteristics of laser-induced acoustic waves in liquids. Journal of Applied Physics 56: 93–95.
89. Pan Y, Birngruber R, Rosperich J & Engelhardt R (1995) Low-coherence optical tomography in turbid tissue: theoretical analysis. Applied Optics 34: 6564–6574.
90. Schmitt JM & Knüttel A (1997) Model of optical coherence tomography of heterogeneous tissue. Journal of the Optical Society of America A 14: 1231–1242.
91. Wang RK (2002) Signal degradation by multiple scattering in optical coherence tomography of dense tissue: a Monte Carlo study towards optical clearing of biotissues. Physics in Medicine and Biology 47: 2281–2299.
92. Thrane L, Yura HT & Andersen PE (2000) Analysis of optical coherence tomography based on the extended Huygens-Fresnel principle. Journal of the Optical Society of America A 17: 484–490.
93. Thrane L (2001) Optical coherence tomography: modeling and applications. Ph.D. dissertation, Risø National Laboratory, Roskilde, Denmark.
94. Andersen PE, Thrane L, Yura HT, Tycho A, Jørgensen TM & Frosz MH (2004) Advanced modeling of optical coherence tomography systems. Physics in Medicine and Biology 49: 1307–1327.
95. Karamata B, Lambelet P, Leutenegger M, Laubscher M, Bourquin S & Lasser T (2005) A semi-analytical model accounting for multiple scattering in optical coherence tomography. Proceedings of SPIE 5690: 386–396.
96. Smithies DJ, Lindmo T, Chen Z, Nelson JS & Milner TE (1998) Signal attenuation and localization in optical coherence tomography studied by Monte Carlo simulation. Physics in Medicine and Biology 43: 3025–3044.
97. Weast RC (Editor) (1974) Handbook of Chemistry and Physics. 55th ed., Chemical Rubber Co., Cleveland, OH.
98. Maier JS, Walker SA, Fantini S, Franceschini MA & Gratton E (1994) Possible correlation between blood glucose concentration and the reduced scattering coefficient of tissues in the near infrared. Optics Letters 19: 2062–2064.
99. Kohl M, Cope M, Essenpreis M & Böcker D (1994) Influence of glucose concentration on light scattering in tissue-simulating phantoms. Optics Letters 19: 2170–2172.
100. Kohl M, Essenpreis M & Cope M (1995) The influence of glucose concentration upon the transport of light in tissue-simulating phantoms. Physics in Medicine and Biology 40: 1267–1287.
101. Liu H, Zhang Y, Kimura M & Change B (1996) Theoretical and experimental investigations on solute-induced changes in optical properties of living tissues. OSA TOPS on Biomedical Optical Spectroscopy and Diagnostics 3: 10–12.
102. Qu J & Wilson BC (1997) Monte Carlo modeling studies of the effect of physiological factors and other analytes on the determination of glucose concentration *in vivo* by near infrared optical absorption and scattering measurements. Journal of Biomedical Optics 2: 319–325.

103. Tuchin VV (Editor) (2002) Handbook of Optical Biomedical Diagnostics. SPIE, Bellingham, Washington, USA.
104. Eskelinen S (1986) Osmotic haemolysis of human erythrocytes, the effect of lysophosphatidylcholine, swelling rate, and temperature. Dissertation, University of Oulu, Finland.
105. Leonardi L & Burns DH (1999) Quantitative measurements in scattering media: photon time-of-flight analysis with analytical descriptors. Applied Spectroscopy 53: 628–636.
106. Kuo IY & Shung KK (1994) High frequency ultrasonic backscatter from erythrocyte suspension. IEEE Transactions on Biomedical Engineering 41: 29–34.
107. van der Heiden MS, de Kroon MGM, Bom N & Borst C (1995) Ultrasound backscatter at 30 MHz from human blood: influence of rouleau size affected by blood modification and shear rate. Ultrasound in Medicine and Biology 21: 817–826.
108. Yoon G, Welch AJ, Motamedi M & van Gemert MCJ (1987) Development and application of three-dimensional light distribution model for laser irradiated tissue. IEEE Journal of Quantum Electronics 23: 1721–1733.
109. Flock ST, Jacques SL, Wilson BC, Star WM & van Gemert MJC (1992) Optical properties of intralipid: a phantom medium for light propagation studies. Lasers in Surgery and Medicine 12: 510–519.
110. van Staveren HJ, Moes CJM, Van Marle J, Prahl SA & van Gemert MJC (1991) Light scattering in Intralipid-10% in the wavelength range of 400-1100 nm. Applied Optics 30: 4507–4514.
111. Troy TL & Thennadil SN (2001) Optical properties of human skin in the near infrared wavelength range of 1000–2200 nm. Journal of Biomedical Optics 6: 167–176.
112. Bondani M, Redaelli D, Spinelli A, Andreoni A, Roberti G, Riccio P, Liuzzi R & Rech I (2003) Photon time-of-flight distributions through turbid media directly measured with single-photon avalanche diodes. Journal of the Optical Society of America B 20: 2383–2388.
113. Zaccanti G, Del Bianco S & Martelli F (2003) Measurements of optical properties of high-density media. Applied Optics 42: 4023–4030.
114. Roggan A, Friebel M, Dörschel K, Hahn A & Müller G (1999) Optical properties of circulating human blood in the wavelength range 400-2500 nm. Journal of Biomedical Optics 4: 36–46.
115. Jacques SL (1996) Origins of tissue optical properties in the UVA, visible and NIR regions. OSA TOPS on advances in optical imaging and photon migration 2: 364–371.
116. Goss SA, Johnston RL & Dunn F (1978) Comprehensive compilation of empirical ultrasonic properties of mammalian tissues. Journal of the Acoustical Society of the America 64: 423–457.
117. Jain NC (1986) Schalm's Veterinary Hematology. 4th edition, Philadelphia: Lea & Febiger.
118. Warwick R & Williams PL (Editors) (1973) Gray's Anatomy. 35th edition, Longman Group Ltd., Edinburgh, Great Britain.
119. Goldshmith LA (Editor) (1991) Physiology, Biochemistry, and Molecular Biology of the Skin. 2nd edition. Oxford University Press, New York, USA.
120. Bussau LJ, Vo LT, Delaney PM, Papworth GD, Barkla DH & King RG (1998) Fibre optic confocal imaging (FOCI) of keratinocytes, blood vessels and nerves in hairless mouse skin in vivo. Journal of Anatomy 192: 187–194.

121. Azzi L, El-Alfy M, Martel C & Labrie F (2005) Gender differences in mouse skin morphology and specific effects of sex steroids and dehydroepiandrosterone. Journal of Investigative Dermatology 124: 22–27.
122. Gilgen HH, Novàk RP, Salathé RP, Hodel W & Beaud P (1989) Submillimeter optical reflectometry. Journal of Lightwave Technology, 7: 1225–1233.
123. Huang D, Swanson EA, Lin CP, Schuman JS, Stinson WG, Chang W, Hee MR, Flotte T, Gregory K, Puliafito CA & Fujimoto JG (1991) Optical coherence tomography. Science 254: 1178–1181.
124. Schmitt JM (1999) Optical coherence tomography (OCT): a review. IEEE Journal of Selected Topics in Quantum Electronics 5: 1205–1215.
125. Drexler W (2004) Ultrahigh-resolution optical coherence tomography. Journal of Biomedical Optics 9: 47–74.
126. Levitz D, Thrane L, Frosz MH, Andersen PE, Andersen CB, Valanciunaite J, Swartling J, Andersson-Engels S & Hansen PR (2004) Determination of optical scattering properties of highly-scattering media in optical coherence tomography images. Optics Express 12: 249–259.
127. Knüttel A, Bonev S & Knaak W (2004) New method for evaluation of *in vivo* scattering and refractive index properties obtained with optical coherence tomography. Journal of Biomedical Optics 9: 265–273.
128. Zhao Z & Myllylä R (2005) Scattering photoacoustic method in measurement of weakly-absorbing turbid suspensions. Proceedings of SPIE, Saratov Fall Meeting, (to be published).
129. Zhao Z & Myllylä R (2005) Measuring the optical parameters of weakly absorbing, highly turbid suspensions by a new technique: photoacoustic detection of scattered light. Applied Optics 44: 7845–7852.
130. Kinnunen M & Myllylä R (2004) Methods for evaluating the optical properties of a material from measured laser pulse shapes. Odimap IV, Oulu, Finland: 340–345.
131. Arridge SR & Schweiger M (1995) Direct calculation of the moments of the distribution of photon time of flight in tissue with a finite-element method. Applied Optics 34: 2683–2687.
132. Hamamatsu (1996) Guide to streak cameras. Cat. No. SSCS1035E02, Japan, 4-5.
133. Liebert A, Wabnitz H, Grosenick D & Macdonald R (2003) Fiber dispersion in time domain measurements compromising the accuracy of determination of optical properties of strongly scattering media. Journal of Biomedical Optics 8: 512–516.
134. Quan KM, MacKenzie HA, Hodgson P & Christison GB (1994) Photoacoustic generation in liquids with low optical absorption. Ultrasonics 32: 181–186.
135. Tam AC & Patel CKN (1979) Optical absorption of light and heavy water by laser optoacoustic spectroscopy. Applied Optics, 18: 3348–3358.
136. Sankaran V, Schönenberger K, Walsh JT Jr & Maitland DJ (1999) Polarization discrimination on coherently propagating light in turbid media. Applied Optics 38: 4252–4261.
137. Popov AP, Priezzhev AV & Myllylä R (2005) Glucose content monitoring with time-of-flight technique in aqueous Intralipid solution imitating human skin: Monte Carlo simulation. Proceedings of SPIE 5862: 251–254.
138. Popov AP, Priezzhev AV & Myllylä R (2005) Effect of glucose concentration in a model light-scattering suspension on propagation of ultrashort pulses. Quantum Electronics 35: 1075–1078.

Original papers

I Kinnunen M, Popov AP, Pluciński J, Myllylä R & Priezzhev AV (2004) Measurements of glucose content in scattering media with time-of-flight technique; comparison with Monte Carlo simulations. Proceedings of SPIE, Saratov Fall Meeting 2003: Optical Technologies in Biophysics and Medicine V 5474: 181–191.

II Kirillin M, Priezzhev AV, Kinnunen M, Alarousu E, Zhao Z, Hast J & Myllylä R (2004) Glucose sensing in aqueous Intralipid suspension with an optical coherence tomography system: experiment and Monte Carlo simulation. Proceedings of SPIE, Optical Diagnostics and Sensing IV 5325: 164–173.

III Kinnunen M, Zhao Z & Myllylä R (2005) Comparison of the pulsed photoacoustic technique and the optical coherence tomography from the viewpoint of biomedical sensing. Proceedings of SPIE, Optical Materials and Applications 5946: 468–480.

IV Kinnunen M, Zhao Z & Myllylä R (2006) Glucose-induced changes in the optical properties of Intralipid. Optics and Spectroscopy 101 (1): 54–59.

V Kinnunen M & Myllylä R (2005) Effect of glucose on photoacoustic signals at the wavelenghts of 1064 and 532 nm in pig blood and intralipid. Journal of Physics D: Applied Physics 38: 2654–2661.

VI Kinnunen M, Myllylä R, Jokela T & Vainio S (2006) In vitro studies toward non-invasive glucose monitoring with optical coherence tomography. Applied Optics 45 (10): 2251–2260.

VII Kinnunen M & Myllylä R (2006) Comparative study of optical coherence tomography, photoacoustic technique, and time-of-flight technique in phantom measurements. Proceedings of SPIE, Saratov Fall Meeting 2005: Optical Technologies in Biophysics and Medicine VII 6163, in press.

Original publications are not included in the electronic version of the dissertation.

233. Karvonen, Sami (2006) Charge-domain sampling of high-frequency signals with embedded filtering

234. Laitinen, Risto (2006) Improvement of weld HAZ toughness at low heat input by controlling the distribution of M-A constituents

235. Juuti, Jari (2006) Pre-stressed piezoelectric actuator for micro and fine mechanical applications

236. Benyó, Imre (2006) Cascade Generalized Predictive Control—Applications in power plant control

237. Kayo, Olga (2006) Locally linear embedding algorithm. Extensions and applications

238. Kolli, Tanja (2006) Pd/Al2O3 -based automotive exhaust gas catalysts. The effect of BaO and OSC material on NOx reduction

239. Torkko, Margit (2006) Maatilakytkentäisten yritysten toimintamalleja. Laadullinen tutkimus resursseista, kehittymisestä ja ohjaustarpeista

240. Hämäläinen, Matti (2006) Singleband UWB systems. Analysis and measurements of coexistence with selected existing radio systems

241. Virtanen, Jani (2006) Enhancing the compatibility of surgical robots with magnetic resonance imaging

242. Lumijärvi, Jouko (2006) Optimization of critical flow velocity in cantilevered fluid-conveying pipes, with a subsequent non-linear analysis

243. Stoor, Tuomas (2006) Air in pulp and papermaking processes

244. György, Zsuzsanna (2006) Glycoside production by in vitro *Rhodiola rosea* cultures

245. Özer-Kemppainen, Özlem (2006) Alternative housing environments for the elderly in the information society. The Finnish experience

246. Laurinen, Perttu (2006) A top-down approach for creating and implementing data mining solutions

247. Jortama, Timo (2006) A self-assessment based method for post-completion audits in paper production line investment projects

248. Remes, Janne (2006) The development of laser chemical vapor deposition and focused ion beam methods for prototype integrated circuit modification

Book orders:
OULU UNIVERSITY PRESS
P.O. Box 8200, FI-90014
University of Oulu, Finland

Distributed by
OULU UNIVERSITY LIBRARY
P.O. Box 7500, FI-90014
University of Oulu, Finland

UNIVERSITY OF OULU P.O. Box 7500 FI-90014 UNIVERSITY OF OULU FINLAND

ACTA UNIVERSITATIS OULUENSIS

ISBN 951-42-8145-4 (Paperback)
ISBN 951-42-8146-2 (PDF)
ISSN 0355-3213 (Print)
ISSN 1796-2226 (Online)